

SYNTHESIS AND STRUCTURAL CHARACTERIZATION  
OF  
NICKEL-BORON NANOALLOYS

A THESIS SUBMITTED TO  
THE GRADUATE SCHOOL OF APPLIED AND NATURAL SCIENCES  
OF  
MIDDLE EAST TECHNICAL UNIVERSITY

BY

LÜTFİYE SEDA MUT

IN PARTIAL FULFILLMENT OF THE REQUIREMENTS  
FOR  
THE DEGREE OF MASTER OF SCIENCE  
IN  
MICRO AND NANOTECHNOLOGY

JUNE 2015



Approval of the thesis:

**SYNTHESIS AND STRUCTURAL CHARACTERIZATION OF  
Ni-B NANOALLOY**

submitted by **LÜTFİYE SEDA MUT** in partial fulfillment of the requirements for  
the degree of **Master of Science in Micro and Nanotechnology Department,**  
**Middle East Technical University** by,

Prof. Dr. Gülbin Dural Ünver \_\_\_\_\_  
Dean, Graduate School of **Natural and Applied Sciences**

Prof. Dr. Tayfun Akın \_\_\_\_\_  
Head of Department, **Micro and Nanotechnology Dept., METU**

Prof. Dr. Amdulla Mekhrabov \_\_\_\_\_  
Supervisor, **Metallurgical and Materials Eng. Dept., METU**

Assoc. Prof. Hande Toffoli \_\_\_\_\_  
Co-Supervisor, **Physics Dept., METU**

**Examining Committee Members:**

Prof. Dr. Vedat Akdeniz \_\_\_\_\_  
Metallurgical and Materials Engineering Dept., METU

Prof. Dr. Amdulla O. Mekhrabov \_\_\_\_\_  
Metallurgical and Materials Engineering Dept., METU

Assoc. Prof. Dr. Hande Toffoli \_\_\_\_\_  
Physics Dept., METU

Assoc. Prof. Dr. Yunus Eren Kalay \_\_\_\_\_  
Metallurgical and Materials Engineering Dept., METU

Dr. Mehmet Yıldırım \_\_\_\_\_  
Materials Science and Engineering Dept., Selçuk University

**Date: -----**

**I hereby declare that all information in this document has been obtained and presented in accordance with academic rules and ethical conduct. I also declare that, as required by these rules and conduct, I have fully cited and referenced all material and results that are not original to this work.**

Name, Last name: Lütfiye Seda Mut

Signature:

## ABSTRACT

### SYNTHESIS AND STRUCTURAL CHARACTERIZATION OF Ni-B NANOALLOYS

Mut, Lütfiye Seda

M.S., Department of Micro and Nanotechnology

Supervisor: Prof. Dr. Amdulla Mehrabov

Co-Supervisor: Doç. Dr. Hande Toffoli

June 2015, 51 pages

Within the scope of this study, it is aimed to produce and to realize the structural characterization of Nickel Boron nanocrystalline/amorphous, alloy/intermetallic phase powders.

Mechanical alloying by high energy ball milling was determined as production method. X-ray diffraction (XRD) for phase analysis, Scanning Electron Microscopy (SEM) for microstructure and morphological analysis, Vibrating Sample Magnetometer (VSM) for change in magnetic properties and Differential Scanning Calorimetry (DSC) for thermal analysis were determined as methods for characterization of produced powders.

Milling operation has been carried out with two different compositions as Ni<sub>80</sub>B<sub>20</sub> and Ni<sub>60</sub>B<sub>40</sub>, prepared from elemental Nickel and Boron powders. For both compositions, after 1, 5, 10, 20, 40, 60 and 80 hours of milling, samples have been taken out and analyses have been carried out. According to the structural analyses, there are no remarkable additional peaks belonging to any intermetallic compounds until 40 hours of milling. For Ni<sub>80</sub>B<sub>20</sub> composition, Ni<sub>3</sub>B and Ni<sub>2</sub>B peaks after 40 hours of milling and for Ni<sub>60</sub>B<sub>40</sub>, Ni<sub>3</sub>B peak after 60 hours of milling were observed notably and with the increase in milling time intensities of these peaks increased.

Besides, XRD and SEM analyses have shown that particle size and/or crystallite size decreased with increasing milling time. Additionally, along with peak broadening in XRD curves, DSC analyses have pointed out the formation of amorphous structure. As for, changes in magnetic properties it was shown that with increase in milling time, saturation magnetization shows a general decrease and hysteresis increases.

**Keywords:** Mechanical Alloying, High-Energy Ball Milling, Nanoalloy, Nanocrystalline Alloy.

## ÖZ

### Ni-B NANOALAŞIMLARININ SENTEZLENMESİ VE YAPISAL KARAKTERİZASYONU

Mut, Lutfiye Seda

Y. Lisans, Mikro ve Nanoteknoloji Bölümü

Tez Yöneticisi: Prof. Dr. Amdulla Mekhrabov

Ortak Tez Yöneticisi: Doç. Dr. Hande Toffoli

Haziran 2015, 51 sayfa

Bu çalışma kapsamında, Nikel Bor nanokristal/amorf, alaşım/intermetalik faz tozların üretilmesi ve karakterizasyonu amaçlanmıştır.

Yüksek enerjili bilye öğütümü ile mekanik alaşımlama, üretim yöntemi olarak seçilmiştir. Üretilen tozların karakterizasyonu amacıyla, faz analizi için X-ışını Kırınımı (XRD), mikroyapı ve morfoloji analizi için Taramalı Elektron Mikroskobu (SEM), manyetik özelliklerdeki değişimin incelenmesi için Titreşimli Örnek Manyetometresi (VSM) ve ısıl analiz için Diferansiyel Taramalı Kalorimetre (DSC) yöntemlerinin kullanılmasına karar verilmiştir.

Öğütme işlemi, elemental haldeki Nikel ve Bor tozlarından hazırlanan,  $Ni_{80}B_{20}$  ve  $Ni_{60}B_{40}$  olmak üzere iki ayrı kompozisyon ile gerçekleştirilmiştir. Her iki kompozisyon için, 1, 5, 10, 20, 40, 60 ve 80 saat öğütmeden sonra örnekler alınarak, analizleri yapılmıştır. Yapısal analizlere göre, 40 saatlik öğütmeye kadar herhangi bir intermetalik bileşiğe ait dikkate değer bir ek pik bulunmamaktadır.  $Ni_{80}B_{20}$  kompozisyonu için,  $Ni_3B$  ve  $Ni_2B$  pikleri 40 saatlik öğütmeden sonra ve  $Ni_{60}B_{40}$  kompozisyonu için,  $Ni_3B$  piki 60 saatlik öğütmeden sonra önemli ölçüde gözlenmiş

ve artan öđütme süresi ile bu piklerin şiddeti artmıştır. Bunun yanında, XRD eğrileri ve SEM analizleri göstermiştir ki, kristalit ve/veya parçacık boyutu, artan öđütme zamanı ile azalmaktadır. Ayrıca, XRD eğrilerindeki pik genişlemesi ile birlikte, DSC analiz sonuçları amorf yapı oluşumunu işaret etmektedir. Manyetik özelliklerdeki değişimlerde ise, artan öđütme zamanı ile doygunluk manyetikliğinin genel bir düşüş gösterdiği ve histeresisin arttığı gösterilmiştir.

**Anahtar Kelimeler:** Yüksek enerjili bilye öđütümü, Mekanik Alaşım, Nanoalaşım, Nanokristal alaşım.

## ACKNOWLEDGEMENTS

I would like to express my sincere thanks to Prof. Dr. Amdulla Mekhrabov and Assoc. Prof. Dr. Hande Toffoli for their precious helps and advices during the development of the study. I would also like to thank Prof Dr. Vedat Akdeniz for his guidance.

I would also like to show gratitude to Dr. Mehmet Yıldırım for his helps and encouraging discussions. I sincerely acknowledge the members of NOVALAB, especially Merve Mediha Karataş for her helps and friendship and to Bengi Yağmurlu and Amir Fadaie.

I also thank to technical and administrative staff of the Metallurgical and Material Engineering Department for their helps and the facilities they have provided.

I am grateful to my parents Semiha Kirazlı Mut and Mücahit Birsoy Mut and to my brother Arma Değer Mut for their endless support and confidence. I am also thankful to my fiance Soner Altın for his continuous encouragement and support. I would also like to thank my friends Burcu Çimen Beşikçioğlu for always standing by me.

## TABLE OF CONTENTS

ABSTRACT.....	v
ÖZ.....	vii
ACKNOWLEDGEMENTS.....	ix
TABLE OF CONTENTS.....	x
LIST OF FIGURES.....	xii
LIST OF TABLES.....	xiv
CHAPTERS	
1.INTRODUCTION AND LITERATURE REVIEW.....	1
1.1. Nanoalloys.....	1
1.2. Applications Of Nanoalloys.....	3
1.2.1. Catalysis.....	3
1.2.2. Applications by Utilization of Magnetic Properties.....	4
1.2.3. Biomedical Applications.....	4
1.2.4. Other Application Areas.....	6
1.3. Mechanical Behavior of Nanocrystalline Metals and Alloys.....	6
1.4. Nickel - Based Alloys.....	7
1.4.1. Ni - Based Alloys Synthesized by Powder Metallurgy.....	9
1.4.2. Ni - Based Nanocrystalline Alloys.....	10
1.5. Ni - B Binary System.....	11
1.5.1. Phase Diagram of the Ni-B Binary System.....	12
1.5.2. Ni-B Nanocrystalline Alloy Synthesis.....	15
1.6. Aim of the study.....	17
2.SYNTHESIS EXPERIMENTS AND STRUCTURAL CHARACTERIZATION	19

2.1. Introduction .....	19
2.2. Mechanical Alloying.....	20
2.2.1. Mechanical Alloying by Ball Milling Process .....	20
2.3. Experimental Method: Milling Pure Nickel Powders.....	23
2.3.1. Milling Process by High Energy Ball Mill .....	24
2.3.2. Characterization.....	24
2.5. Experimental Method: Milling Nickel-Boron Powders .....	25
2.5.1. Milling Process by High Energy Ball Mill .....	25
2.5.2. Characterization.....	26
3.RESULTS AND DISCUSSIONS.....	27
3.1. Milling of Pure Nickel Powders.....	27
3.2. Milling of Nickel Boron Powders .....	33
4.CONCLUSION.....	45
REFERENCES .....	47

## LIST OF FIGURES

### FIGURES

Figure 1. A summary of major considerations for potential biomedical.....	5
Figure 2. Ni-B Phase Diagram (Weil & Parker, 1990) .....	12
Figure 3. Schematic demonstration of CFe <sub>3</sub> type for a) a single unit cell b) eight unit cells (Brandon & Kaplan, 2013).....	13
Figure 4. Composition range for amorphous phase formation in the Ni-B binary system .....	14
Figure 5. Schematic view of ball and powder mixture (Lü & Lai, 2013) .....	21
Figure 6. Fusing and fracturing process during ball milling (Schwartz, 2002) .....	22
Figure 7. Fritsch Pulveriste 7 Premium Line High Energy Ball Mill, stainless steel	23
Figure 8. XRD patterns, for initial and milled pure Nickel powders for different time periods.....	27
Figure 9. Detailed XRD patterns of initial and milled pure Ni powders for different time periods .....	28
Figure 10. SEM images of (a) unmilled pure Ni powders and powders milled for (b)1 h, (c)5 h, (d)10 h, (e)20 h.....	30
Figure 11. Hysteresis curves of unmilled pure Ni powders and Ni powders milled for 1, 5, 10 and 20 h .....	31
Figure 12. Change in saturation magnetization, remanent magnetization and coercivity against unmilled and milled pure Ni powder for different time intervals.....	32
Figure 13. XRD curves of Ni <sub>80</sub> B <sub>20</sub> , initial powders and powders ball milled for 1, 5, 10, 20, 40, 60 and 80 h.....	33
Figure 14. XRD curves of Ni <sub>80</sub> B <sub>20</sub> in detail for milled powder for 40, 60 and 80 h.	34
Figure 15. XRD curves of Ni <sub>60</sub> B <sub>40</sub> , initial powders and powders ball milled for 1, 5, 10, 20, 40, 60 and 80 h.....	34

Figure 16. XRD curves of Ni <sub>60</sub> B <sub>40</sub> in detail for milled powder for 40, 60 and 80 h	35
Figure 17. SEM images for Ni <sub>80</sub> B <sub>20</sub> composition powder milled for (a) 0 h (initial), (b) 1 h, (c) 5 h, (d) 10 h, (e) 20 h, (f) 40 h, (g) 60 h, (h) 80 h	37
Figure 18. SEM images for Ni <sub>60</sub> B <sub>40</sub> composition powder milled for (a) 0 h (initial), (b) 1 h, (c) 5 h, (d) 10 h, (e) 20 h, (f) 40 h, (g) 60 h, (h) 80 h	38
Figure 19. High Resolution SEM images for Ni <sub>80</sub> B <sub>20</sub> composition powder milled for (a) 60 h (b) 80 h	39
Figure 20. High Resolution SEM images for Ni <sub>60</sub> B <sub>40</sub> composition powder milled for (a) 60 h (b) 80 h	39
Figure 21. DSC analyses of the initial and milled powder for 20 h for Ni <sub>80</sub> B <sub>20</sub> sample	40
Figure 22. DSC analyses of the initial and milled powder for 20 h for Ni <sub>60</sub> B <sub>40</sub> sample	41
Figure 23. Hysteresis curves for initial Ni <sub>80</sub> B <sub>20</sub> powder and powders milled for different time periods.	41
Figure 24. Hysteresis curves for initial Ni <sub>60</sub> B <sub>40</sub> powder and powders milled for different time periods	43

## LIST OF TABLES

### TABLES

Table 1. Crystallographic data of Ni-B binary system (Taskinen & Teppo, 1993), (Villars, 1998).....	12
Table 2. The crystallite sizes, calculated by the Scherrer equation, changing by milling time .....	29
Table 3. Magnetic parameter values of initial Ni powders and Ni powders milled for 1, 5, 10 and 20 h .....	31
Table 4. The crystallite sizes, calculated by the Scherrer equation, changing by milling time .....	36
Table 5. Magnetic properties of initial Ni <sub>80</sub> B <sub>20</sub> powder and powders milled for different time periods.....	42
Table 6. Magnetic properties of initial Ni <sub>60</sub> B <sub>40</sub> powder and powders milled for different time periods.....	43

## CHAPTER 1

### INTRODUCTION AND LITERATURE REVIEW

#### 1.1. Nanoalloys

A great number of properties can be obtained and improved in metallic systems by getting combinations of different components to produce alloys and intermetallic compounds. Alloy nanoparticles, in other words nanoalloys are multicomponent metallic particles having diameter size range between 1-100 nm. Following the development of nanotechnology, with the ability to control the atoms and molecules through different ways, there has been an increase in the unique properties obtained from materials and nanoalloys.

Nanoalloys have remarkably diverse range of physical properties, containing corrosion resistance, shape-memory effects, ferromagnetism, superconductivity, catalytic activity, structural hardness and so they have the potential to be used in many applications.

There are several reasons of interest in nanoalloys. The most important reason is that properties of them can be adjusted by changing atomic ordering and/or composition. Another significant reason is being the properties of metal and alloy nanoparticles depend on size. Optical, magnetic and electronic properties, structural forms and chemical reactivity are a function of size and composition. Depending on size, numerous features may be obtained (Jellinek, 2008). Alloy nanoparticles may exhibit properties which are different from the bulk form of the same alloys. As an example for that, Peng et. al. (Peng & Yang, 2008) indicated that, while platinum and silver cannot form a solid solution with the composition between about  $\text{Ag}_2\text{Pt}_{98}$  and  $\text{Ag}_{95}\text{Pt}_5$  at a definite miscibility gap at 400 °C or below in bulk form, alloy

particles and wires can be made within the same miscibility gap at the nanometer scale. Another example is the change in magnetic behaviours with size such as ferromagnetic small Rh clusters in contrast to the paramagnetic bulk form of the same element (Reddy, Nayak, Khanna, Rao, & Jena, 1999).

Regardless of size, nanoalloys may also display features together that are different than that of elemental components. For instance, in catalysis by bimetallic nanoalloys synergistic effect may occur. Pd-Pt for aromatic hydrocarbon hydrogenation and Ru-Pd that have a better catalytic activity and selectivity than that of pure Ru or Pd, are some examples that synergistic effects have been observed. Moreover, “a clear synergistic effect has been observed in the catalytic hydrogenation of crotonic acid to butanoic acid by bimetallic  $\text{Pt}_{0.2}\text{Rh}_{0.8}$  colloids” (Ferrando, Jellinek, & Johnston, 2008).

One of the important parameters that affect the physical and chemical properties of a nanoparticle is chemical mixing and the possibilities are quite diverse. The same set of metals A and B may form different structures, depending on the elements, thermal conditions and details of the synthesis procedure (Mejía-Rosales, Ponce, & José-Yacamán, 2013): mixtures, core-shell nanoparticles (Schärftl, 2010) , Janus nanoparticles (B. Wang, Li, Zhao, & Li, 2008), onion-like nanoparticles (Mariscal, Oldani, Dassie, & Leiva, 2008) or combinations of these types of structures. Also, including the shape of the particle in the scene, makes the possibilities of variations for a nanoalloy very much. In addition, the extra ordinary interest of nanoalloy researches on compositions, segregation properties and surface structures is because they are significant parameters affecting catalytic activity and chemical reactivity.

Depending on the changes in composition and structure of nanoalloys, only slight alterations may occur in properties of nanoalloys or they may show very significant changes in behavior. Since, researches on this matter are not sufficient to understand all the relationships between structure and properties of numerous combinations of nanoalloys, more studies are needed on this point.

Because of all notable properties mentioned, nanoalloys have become the materials utilized for various purposes already, and they seem to be used in more areas with their promising features.

## **1.2. Applications Of Nanoalloys**

Due to their novel properties, nanoalloys have already been utilized for diverse scientific, technological and industrial use. Some of the main application areas are catalysis, magnetic applications and biomedicine.

### **1.2.1. Catalysis**

Nanoalloy catalysis is a highly important and promising topics of nanotechnological researches. Important reasons for that are the size and composition dependence of the chemical reactivity of nanoalloys and their extraordinary surface activity. Nanoalloys are favorable as candidates for catalysts with their fine-tuned properties affecting chemical reactivity.

The use of nanoalloys in catalysis is an area of interest and one of the most common application areas. It has been shown that the catalytic activity of a metal can be improved by mixing two or more metals forming nanoalloys. In addition, by mixing various metals, the structure, morphology and hence the chemical properties of the nanoparticles can be tuned in a variety of possibility, so spectrum of reactive possibilities can be substantially widened.

Up to the present, quite a number of metal pairs have been explored already. These include, “Co–Ni (for growth of carbon nanotubes), Co–Pt and Ru–Pt (for fuel cell electrocatalysis), Pd–Pt (for use in catalytic converters), Pd–Au (for formation of H<sub>2</sub>O<sub>2</sub> from H<sub>2</sub> and O<sub>2</sub>; CO and alcohol reduction; and synthesis of vinyl acetate); Ru–Pd (for single-step hydro-genation); as well as Ni–Pd, Ni–Pt, Ni–Au, Cu–Pd, Cu–Pt, Pt–Au, Mo–Pt, Rh–Pt and Re–Ir” that most of them having superior catalytic properties (Jellinek, 2008).

Palladium and platinum metals are the most widely used and studied catalysts, but they are expensive. Hence, the usage of inexpensive metals like Ni, Co, Cu by alloying with Pd and Pt, is preferred to reduce the cost. Ni-Pd nanoalloy catalysts being used in the hydrogenation of nitrogen substituted aromatic compounds (Raja et al., 2005) and Ni-Pt that are used for oxygen reduction in fuel cells, as electrocatalysts (Toda, 1999) are some common examples.

### **1.2.2. Applications by Utilization of Magnetic Properties**

The most common magnetic elements are nickel (Ni), iron (Fe), and cobalt (Co) or mixtures of them. Magnetic materials can be manipulated by a magnetic field. Interest in magnetic nanoalloys has increased recently since they have unique properties and because these properties can be utilized in various applications such as magnetic separation, magnetic recording media, data storage (Frey & Sun, 2009), sensors and biomedicine (Leung, 2013).

Additionally, bimetallic nanoalloys have been produced by embedding magnetic metals into nonmagnetic metals. Giant magneto-resistance (GMR) materials have potential applications, as well. As magnetic nanomaterials exhibit different magnetic properties when compared to the bulk forms such as coercivity, researches carried on for them. When 3d metals and 5d metals are combined as it is at Fe-Pt and Co-Pt, the nanoalloys occurred exhibit high magnetic anisotropy with associated high magnetic susceptibility and coercivity. This makes them good candidates for ultrahigh density magnetic recording media.

### **1.2.3. Biomedical Applications**

In contrast to the other application areas, for biomedical implementations there are concerns limiting the usage of nanoalloys. The main concerns are toxicity and biocompatibility. Information on the use of nanoalloys in biology or medicine is less often than other fields.

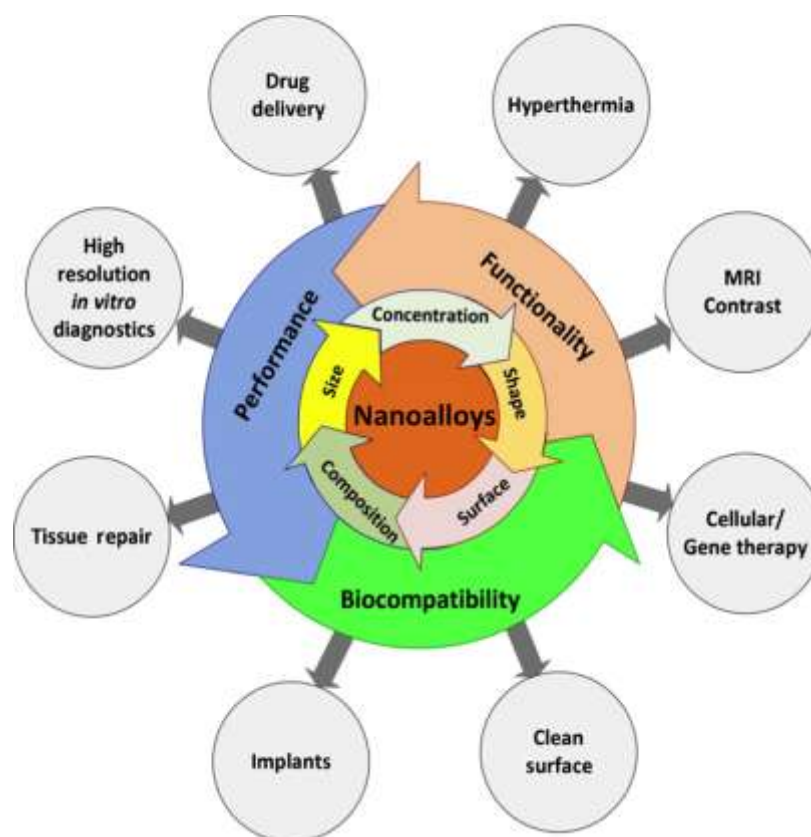


Figure 1. A summary of major considerations for potential biomedical applications of nanoalloys (McNamara & Tofail, 2013).

Concerning various parameters and according to the intended end use properties diverse implementation areas are possible by different alloy combinations (Figure 1). Among limited researches on the use of nanoalloys in biomedicine; magnetic properties of nanoalloys has been focused on such as nuclear magnetic resonance (NMR) imaging, drug and gene delivery, hyperthermia, MRI contrast enhancement and fluorescent biological labeling.

Fe-Pt and Fe-Co nanoalloys are some remarkable examples that have been researched for biomedical applications due to their superparamagnetism and a high X-ray absorption coefficient which makes them ideal candidates for MRI contrast agents and magnetic drug delivery carriers. NiTi also known as nitinol is also another example used in biomedicine due to its unique properties such as shape memory effect, biocompatibility, corrosion resistance and superelasticity (McNamara & Tofail, 2013).

#### **1.2.4. Other Application Areas**

It is expected that with the increasing number of researches leading to the development of controlled synthesis procedures and to the determination of magnetic, catalytic and biomedical properties of the nanoalloys which are the main interest in utilizations there will be more applications in the future.

According to some projections (Ferrando et al., 2008) it is foreseen about the future of nanoalloys that, “on the technological side, advances in fine tuning of nanoalloy properties by controlled doping will facilitate a wide range of applications and make nanoalloy-based nanodevices a reality. Experimental and theoretical studies will also be extended to tailored 1D, 2D, and 3D nanoarchitectures constructed from nanoalloy building blocks.” Additionally, “expansion of the area to tri- and multimetallic nanoalloys as well as heterogeneous particles, such as alloyoxide composites and functionalized hybrid bionanoalloy particles for medical applications” is expected. Besides, developments in computations is expected to facilitate complex theoretical nanoalloy studies become easier and faster. Furthermore, with the increasing number of studies, applications of new technologies is anticipated to become more feasible and common. On the whole, nanoalloys seem to be used in more and more technological applications in the near future.

#### **1.3. Mechanical Behavior of Nanocrystalline Metals and Alloys**

There are a number of methods at laboratory-scale to synthesize nanocrystalline and ultrafine crystalline materials. These techniques can be classified into the following groups: mechanical alloying (Koch, 1997), (Zhou, Liao, Zhu, Dallek, & Lavernia, 2003), (Zhang, Wang, Scattergood, Narayan, & Koch, 2003), severe plastic deformation (Valiev & Alexandrov, 2002), electrodeposition (Erb, 1995) and gas-phase condensation (Eastman & Weertman, 1997). Different mechanical properties of materials obtained through various ways have also been studied previously.

The mechanical properties of fully-dense FCC metals (Ni, Cu and Pd) with grain size less than 100 nm obtained from uniaxial tension/compression tests and micro- or

nanoindentation indicated that “typically, these nanocrystalline metals exhibit significantly higher yield strength, and reduced tensile elongation relative to their microcrystalline counterparts.” As for the strain rate effects in compression, tension and indentation, previous studies have shown that “nanocrystalline metals exhibit highly strain-rate sensitive mechanical response under different loading conditions” (Kumar, Van Swygenhoven, & Suresh, 2003).

In brief, when compared to conventional metals, nanocrystalline metals have numerous interesting mechanical properties like high hardness, high strength and good resistance performance to wear and corrosion. However, for any specific application, whether the material satisfies the need of certain minimum acceptable level in terms of damage tolerance which can make other properties useless, should be considered.

#### **1.4. Nickel - Based Alloys**

Nickel is an element that has been in use for centuries, however its actual discovery dates back to the 18th century. Ni is a hard metal which has resistance to corrosion and outstanding strength. Its electricity and heat conductivity is low. One of the major uses of nickel is the preparation of alloys. Nickel alloys are especially precious for their strength and resistance to corrosion.

Ni based alloys have significant resistance to extreme corrosion and wear like Ni. Because of physical properties of Ni alloys, they can be utilised in applications that require; magnetic properties, high resistance to wear and high strength especially at high temperatures. Some major applications of Ni and Ni based alloys are:

- Chemical and petrochemical industries: bolts, fans, valves, reaction vessels, tubing, transfer piping, pumps.
- Pulp and papermills: tubing, doctor blades, bleaching circuit equipment, scrubbers.

- Aircraft gas turbines: disks, combustion chambers, casings, shafts, bolts, exhaust systems, blades, vanes, burner cans, afterburners, thrust reversers.
- Steam turbine power plants: bolts, blades, stack gas reheaters.
- Reciprocating engines: Turbo chargers, exhaust valves, hot plugs, valve seat inserts.
- Metal processing: hot-work tools and dies.
- Medical applications: dentistry uses, prosthetic devices.
- Space vehicles: aerodynamically heated skins, rocket engine parts.
- Heat treating equipment: trays, fixtures, conveyor belts, fans, baskets, furnace mufflers.
- Nuclear power systems: control rod drive mechanisms, valve systems, springs, ducting.
- Pollution control equipment: scrubbers, flue gas desulfurization equipment (liners, fans, stack gas reheaters, ducting).
- Metal processing mills: ovens, afterburners, exhaust fans.
- Coal gasification and liquification systems: heat exchangers, repeaters, piping,.
- Automotive industry: spark plugs, glow plugs (in diesel engines), catalytic converters (Davis, 2000a).

Other utilizations of Nickel are machinery and household applications, transportation and construction.

Nickel can be electroplated onto other metals to form a protective coating. Nickel based alloys have been used for surface engineering applications by coating and make considerable contributions to protection of materials. Nickel plating is widely applied for industry, electroforming and household applications. Electroless nickel coating are done by chemical reduction of Ni ions from an aqueous solution. There are three types of electroless coatings: Nickel - Phosphorus, Nickel- Boron and composite coatings including different combinations like Ni – P and fluorocarbons, silicon carbide. For thermal spray coating, atomized Nickel alloy powders (including Nickel Chromium Borides and Carbides) are deposited through various thermal

spray techniques. This method is used for wear-resistant implementations. Weld overlay coatings are implemented for either wear resistant applications (hardfacing alloys including nickel based/boride alloys) or corrosion resistant purposes (Davis, 2000b).

Ni based alloys have also other application areas utilizing their unique physical properties including shape memory behaviour, soft magnetic alloys, low expansion and so on.

#### **1.4.1. Ni - Based Alloys Synthesized by Powder Metallurgy**

Powder metallurgy is defined as to generate metal powders and to obtain finished materials from pure, mixed or alloyed metal powders. Non-metallic materials also can be added. The major steps in powder metallurgy are powder production, compaction, sintering and finishing operations (heat treating, steam treating etc.). At powder manufacturing phase, production of finer powders and even nanocrystalline materials (10-100 nm grain size) to obtain enhanced properties is a recent trend and area of interest (Angelo & Subramaian, 2008).

Powder processing techniques are widely used in nickel based superalloy production. Forging superalloys and weakly forgeable materials may be difficult for a metal forging process. For instance, forging of high-strength gas turbine disk alloy compositions are difficult, therefore they are powder processed instead. For powder generation inert atmospheres are preferred. Powders are compacted via hot isostatic pressing (which is the simultaneous application of high temperature and pressure) or extrusion. Easy grain size control and minimum segregation are important advantages of powders processing. Additionally, by powder metallurgy, low gas content can be maintained to minimize the defects.

For turbine blades and tubings of heat exchangers requiring high temperatures alloys strengthened by oxide dispersion which is addition of oxide powders between alloy layers are used. The main method to produce these kind of materials is mechanical alloying (Davis, 2000c).

### 1.4.2. Ni - Based Nanocrystalline Alloys

When previous studies are examined it is seen that from various synthesis methods to the properties (such as arrangement, magnetic properties, catalytic activity etc.) there are diverse researches about Ni - based nanocrystalline alloys.

Ni-Pt nanoalloys were obtained via radiolytic synthesis and other methods (Belloni, Mostafavi, Remita, Marignier, & Delcourt, 1998), (Schaak et al., 2005) . Nunomura and co-workers have developed a chemical procedure including the reduction of Pd by Ni ion, produced Pd/Ni nanoalloys at different Ni concentrations, investigated the magnetic properties and reported that “Ni concentration dependence on magnetization reveals the existence of a giant magnetic moment effect, where the critical concentration of 6.3 at% is higher than the bulk state one” (Nunomura, Hori, Teranishi, Miyake, & Yamada, 1998).

Ni-Cu having nanocrystalline structure has been obtained through various ways such as mechanical alloying (Pabi, Joardar, Manna, & Murty, 1997) and electrodeposition (Kamel, Anwer, Abdel-Salam, & Ibrahim, 2014).

In the scope of their research, Portales et al. (Portales et al., 2002) have investigated the structural arrangement of Ni – Ag nanoparticles within Al matrix and they reported that “Raman results are in agreement with a core-shell structure of the nanoparticles, the silver shell being loosely bonded to the nickel core”.

Sondón et al. (Sondón, Guevara, & Saúl, 2007) have studied on Ni-Rh clusters and calculated the magnetic properties by solving Hamiltonian and related segregation behavior to the magnetic properties. They reported about the relationship between Rh content and magnetic behaviour that “for low Rh concentrations, there is an enhancement of the total magnetic moments mainly due to surface effects. In the central zone of concentrations, the resulting magnetic moments are a combination of hybridization and size reduction effects” and “for concentrations above 76% Rh, the Ni-Rh coordinations are so low that it leads to negligible total magnetic moments for the clusters”.

Sub-nanometer scale Ni-Al particles are synthesised by Massicot et al. (Massicot, Schneider, Fort, Illy-Cherrey, & Tillement, 2000) with reduction reaction of  $\text{Ni}(\text{OAc})_2$  and  $\text{Al}(\text{OAc})_3$  and investigated the catalytic activity of them and reported for the resulting nanoparticles that they “exhibit high catalytic activity for the reductive dehalogenation of aliphatic and aromatic halides and polychlorinated arenes”.

### **1.5. Ni - B Binary System**

Chen et. al (C. ; Chen, Bai, Chen, & Xuchu, 2013) have studied the impact of Boron on properties and structures of Ni - B binary system alloys.

Boron influence on structures and properties in nickel-based alloys has been investigated by and found that intermetal compounds that is boride are the phases that affect wear resistance and hardness notably. Furthermore, Diabb et al. reported that 3.5 wt% of Boron increases wear resistance above one order of magnitude (Diabb et al., 2009).

Because of the boride dispersion within the microstructure, boride containing nickel base alloys exhibit a good resistance to abrasion. Low- stress abrasion resistance usually enhances with boron content. Additionally, boride containing nickel base alloys have moderate resistance to galling (Davis, 2000d).

Researches on NiB alloy film has shown that, it is a very soft magnet which makes it a good candidate for applications as magnetic recording media (Glass, Kher, Kim, Dowben, & Spencer, 1990).

Boride containing nickel-base alloys are one of the most commercially available nickel-base hardfacing alloys. Hardfacing is a process that tougher material is added to the main metal. The boride containing nickel-base alloys were commercially produced for the first time as spray and fused powders. Some of the examples of these alloys being currently available are bare cast rod, tube wires, powders for plasma weld and manual torch.

### 1.5.1. Phase Diagram of the Ni-B Binary System

Phase diagram of Ni-B binary system is given in Figure 2.

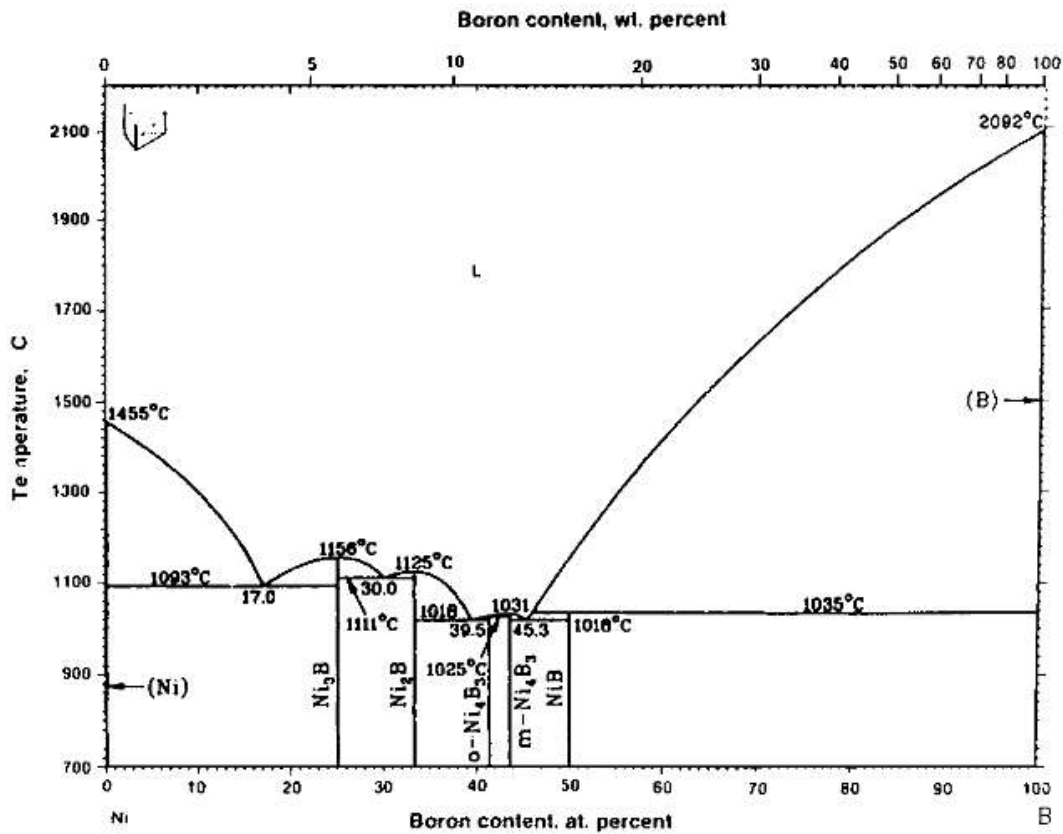


Figure 2. Ni-B Phase Diagram (Weil & Parker, 1990)

As it is seen from the phase diagram given above, within Ni-B binary system there are four eutectic compositions possible and five intermetallic compounds. Crystallographic data of Ni-B binary system including these intermetallics are given in Table 1.

Table 1. Crystallographic data of Ni-B binary system (Taskinen & Teppo, 1993), (Villars, 1998)

Phase	Structure	Type
(Ni)	Face Centered Cubic (FCC)	Cu
Ni <sub>3</sub> B	Orthorombic	CFe <sub>3</sub>

Table 1 (continued)

Phase	Structure	Type
$\text{Ni}_2\text{B}$	Tetragonal	$\text{Al}_2\text{Cu}$
$\text{Ni}_4\text{B}_3$ (o)	Orthorombic	$\text{B}_3\text{Ni}_4$ (o)
$\text{Ni}_4\text{B}_3$ (m)	Monoclinic	$\text{B}_3\text{Ni}_4$ (m)
$\text{NiB}$	Orthorombic	$\text{BCr}$
(B)	Rhombohedral	B

For the  $\text{Ni}_3\text{B}$  intermetallic compound, schematic drawing of its type  $\text{CFe}_3$  can be seen in Figure 3.

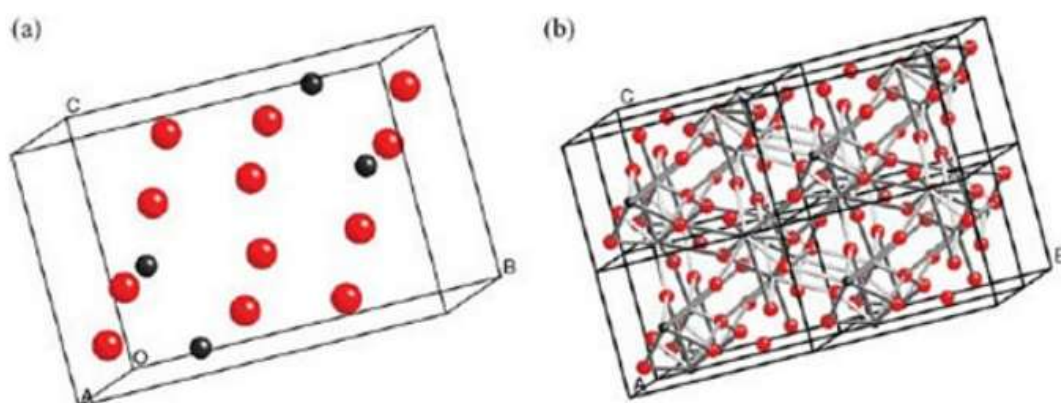


Figure 3. Schematic demonstration of  $\text{CFe}_3$  type for a) a single unit cell b) eight unit cells (Brandon & Kaplan, 2013)

Inoue et. al. (Inoue, Akihiro, & Tsuyoshi, 1979) investigated Ni-B amorphous alloys with high boron concentration. The composition range for amorphous phase formation without any traces of crystalline phase within the Ni-B binary system they reported is given in the following figure. They reported with this figure that the amorphous formation is limited to the range between 33 and 43 of B% for the system.

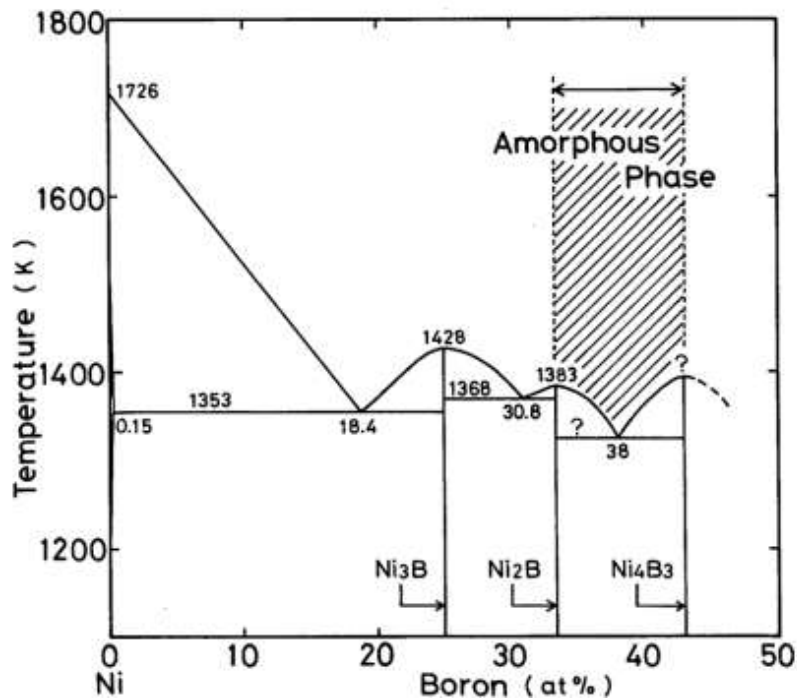


Figure 4. Composition range for amorphous phase formation in the Ni-B binary system

There are a number of researches on Ni-B amorphous alloys. Campbell et. al. (Campbell, Barbour, Hills, & Nastasi, 1989) reported in 1989 that “an amorphous Ni-B alloy was formed at the interfaces between layers of polycrystalline nickel and amorphous boron during electron-beam deposition of Ni/B/Ni trilayer structures. It has been shown for the first time that an amorphous metal-boron alloy is produced by thermal solid state amorphization reaction”.

Through chemical reduction of Ni ions together with  $\text{KBH}_4$ , amorphous Ni-B alloys composed of different B contents have been prepared by Hui et. al (Hui Li, Li, Dai, Wang, & Fang, 1999). According to the results of experiments they indicated that with the increasing B content amorphous degree of the alloy enhanced.

Li et. al. prepared samples of Ni-B and Ni-P amorphous alloy by chemical reduction with  $\text{BH}_4^-$  or  $\text{H}_2\text{PO}_2^-$ . Then, they compared both alloys and reported that at Ni - P there is no important electron transfer whereas B gives electron to Ni and explained

this as the reason for the difference between the catalytic behaviours of these two alloys (Hexing Li, Li, Dai, & Qiao, 2003).

Another research on Ni – B catalysts belongs to Geng et. al. (Geng, Jefferson, & Johnson, 2007). They claimed that Ni – B catalyst has an unusual structure. Although according to the previous suggestions the structure is amorphous they stated that “it is not amorphous but actually possesses a highly unusual nanostructure which is made up of tiny nickel crystallites (1–3 nm) bound in the matrix of boron-containing species” and “boron acts to “cement” the crystallites together and prevents their subsequent sintering”. and interpreted the results as an explanation for the high activity of Ni – B for hydrogenation catalysis because of the large surface area.

### **1.5.2. Ni-B Nanocrystalline Alloy Synthesis**

Legrand et. al. (J. Legrand , A.Taleb, S. Gota , M.J. Guittet, 2002) obtained nanoparticles, via reduction by sodium borohydride at different atmospheric conditions (under nitrogen and air). Consequently, under nitrogen, they produced Ni<sub>2</sub>B intermetallic compound and in open air they obtained Ni and Ni–B mixture. In addition, they reported the significant difference at magnetic properties of these two samples.

Destree et. al. (Destrée & Nagy, 2006) have studied the preparation of inorganic nanoparticles including Ni<sub>2</sub>B using microemulsions, as a function of the concentration of the precursor molecules, the size of the inner water cores and the manner of mixing the various solutions. They reported the dependence of the nanoparticle size on the various physicochemical parameters. They pointed out that either a monotonous increase of the size or the presence of a minimum was observed as a function of the concentration of the precursor molecules.

NiB nanoparticles in water-in-oil microemulsions and their catalysis during hydrogenation of carbonyl and olefinic groups were also prepared by Chiang et. al. The ME-NiB samples were characterized by XRD as an amorphous structure and by Transmission Electron Microscopy (TEM) analysis as having particle size

distributions in the range 3–8 nm, being much smaller than that of NiB (20–50 nm) prepared by the typical chemical reduction method (Chiang, Liaw, & Chen, 2007). Amorphous NiB catalysts are typically prepared by the chemical reduction method with NaBH<sub>4</sub> in an aqueous or ethanolic solution (Y. Chen & Chen, 1994), (Y. Chen, Liaw, & Chiang, 2005).

Nano-amorphous Ni–B alloys is an area of interest as a catalyst because of its high activity and selectivity. To understand well and modify the catalytic properties of nano-amorphous Ni–B alloys, many studies have been carried out about the role of boron, catalytic properties, models of catalytic sites and the structural evolutions in the catalytic process for nano-amorphous Ni–B alloys (Hui Li, Ding, Wang, Zhang, & Bian, 2001), (Y. Chen et al., 2005).

Wang et. al. have researched hydrogen storage in a Ni–B nanoalloy-doped three-dimensional graphene material (Y. Wang, Guo, et al., 2011). Later on, in another study, two-dimensional graphene material is doped with Ni-B nanoalloys via a chemical reduction method. The measured adsorption isotherms of hydrogen and nitrogen suggested that the Ni-B nanoalloys function as catalytic centers to induce the dissociative adsorption of hydrogen (spillover) on the graphen. Consequently, Ni-B nanoalloys without using any noble metal found as a promising catalyst for hydrogen storage application (Y. Wang, Liu, et al., 2011).

Despite, all the potential uses and advantages of NiB nanoalloys, there are not so many researches on the subject, especially for mechanical alloying of NiB by ball milling. Corrias et. al. (Corrias, Ennas, Musinu, Paschina, & Zedda, 1995) have reported their research on the preparation of nanocrystalline nickel boride powders via solid state reaction induced by the ball milling of Ni-B mixtures, in 1995. They (Corrias, Ennas, Marongiu, et al., 1995) also investigated different energetic conditions affecting the rate of the process such as milling rotation speed and ball diameter, reported in another research.

## **1.6. Aim of the study**

Bi- and multi-metallic nanoparticles, namely nanoalloys have very complex structures and properties that highly depend on their size, composition and ordering. They can be tailored for various scientific and industrial applications. New methodologies and results for development, characterization and production of different nanoalloys are important as it could be lead to new materials, novel properties and diverse applications.

Although Ni-B alloys have advantages and superiorities such as high activity and selectivity as a catalyst, utilizable magnetic properties etc. there are not so many researches on Ni-B nanoalloys and particularly on mechanical alloying by ball milling of Ni-B.

Within the scope of this study, it is aimed to produce Ni-B crystalline / amorphous nanocomposite powders by high energy ball milling and to realize the structural characterization varying by milling time. Furthermore, to obtain a relationship between size, structure, morphology and magnetic properties is aimed.



## CHAPTER 2

### SYNTHESIS EXPERIMENTS AND STRUCTURAL CHARACTERIZATION

#### 2.1. Introduction

There are different types of methods to synthesize nanostructured materials. These production methods are classified in two main classes as bottom-up and top-down approaches. Basically, whereas bottom up approach including the methods like molecular beam epitaxy, chemical vapor deposition, sol-gel synthesis etc. refers assembling of single atoms or molecules into larger structures; top down approaches including methods like lithography, ball milling etc. implies breaking down of large particles of a material to obtain nanostructures from them.

Among the top-down approaches, high energy ball milling is one of the most effective, simple and low-cost method and it can be used for synthesis of various nanostructured materials, nanocrystalline alloys, and nanocomposites. Mechanical alloying is a powder metallurgy processing technique including repeated cold welding, fracturing and rewelding of powder particles in a high-energy ball mill. Mechanical alloying defines a process that pure elemental powders, compounds or or alloys are ground together. In case the powders are pure metals; solid solution, intermetallic, or amorphous phase may occur. In this technique, as particle size decreases, grinding operation generates microdeformation of the crystal lattice of the ground material. Therefore, as well as smaller particle sizes, smaller crystallite sizes can be obtained. Also amorphous structure which is desirable for various applications may be obtained.

## **2.2.Mechanical Alloying**

Mechanical alloying is extensively used to generate alloy nanoparticles or alloy powders composed of metal – metal or metal – metal binary systems (Fadaie, Mekhrabov, & Akdeniz, 2014), (Joardar, Pabi, & Murty, 2007), (Murty & Rao, 1995), (Murty, 1992). By ball milling, initial elements intermix at an atomic level through a solid state reaction and the result of this process may be in a different phase such as amorphous or crystalline or a mixture of both.

The utilization of mechanical alloying started in 1960 with the production of Ni-based superalloys which is strengthened with oxide dispersion by the purpose of having high strength at different temperatures and this technique is now widely used to generate diverse alloys having various physical structures, hence various physical properteis (Suryanarayana, 2008).

Being able to use all types of materials is an important advantage of mechanical alloying. Another significant reason for mechanical alloying by ball milling to be a preffered method to obtain nanocrystalline materials is its simplicity. Moreover, on the laboratory scale, it is a relatively cheap method because of inexpensive equipments when compared to the other methods. Additionally, mechanical alloying by ball milling is a process that can be applied to the industrial applications easily, as it can be scaled up. Therefore, it is a highly prefferable method for industrial utilizations, as well (Koch, 1997). All in all, mechanical alloying by ball milling has proved its ability to be an economical and effective way to produce nano-crystalline materials.

### **2.2.1. Mechanical Alloying by Ball Milling Process**

The ball milling method is based on powder – ball collision. Powder particles are surrounded by the colliding balls during the milling operation and deformation and/or fracture occurs. According to the mechanical behaviour of the powder components and their phase equilibria, final structure appears. A simple schematic

view of ball mill that shows the movements during operation is given in the following figure.

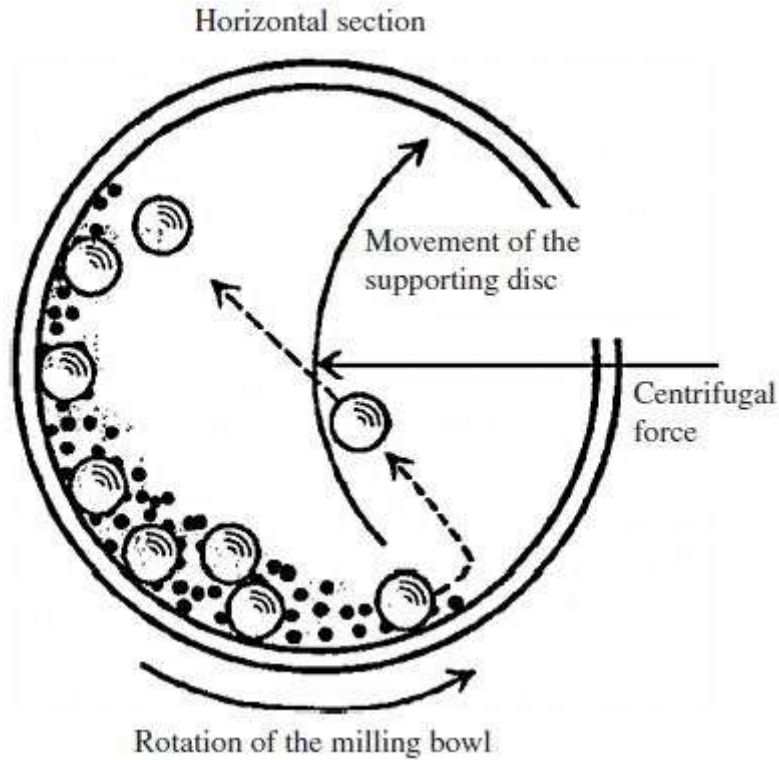


**Figure 5.** Schematic view of ball and powder mixture (Lü & Lai, 2013)

Under the forces due to the different movements of the bowl, powders get influenced by the balls. Everytime two balls collide, powder particles are trapped between these balls. Hence, particles are deformed. The alloying is affected by the powder - ball collisions in a few steps. Initially, intense cold welding is significant. Then, particles get hardened and fracturing and following the fracturing cold welding occurs and finer particles are obtained. Microstructures also gets finer and solid solution starts to form. At last, a steady state phase occurs. Up to the process finishes, highly deformed metastable phases exist. Usually, at the end of the process steps microstructure is below  $\mu\text{m}$  size.

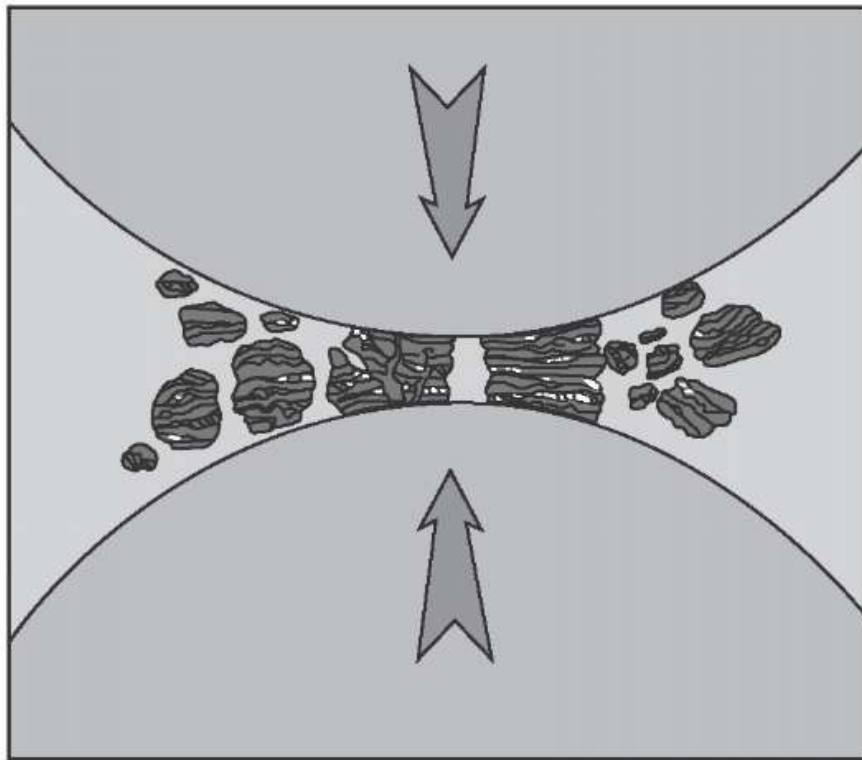


**Figure 6.** Fusing and fracturing process during ball milling (Schwartz, 2002)

Ball milling experiments for this study has been carried out with Fritsch Planetary Micro Mill Pulveristte 7 Premium Line in Novel Alloys Design and Development Laboratory (NOVALAB). Working principle of the Fritsch Planetary Micro Mill Pulveristte 7 Premium Line ball mill equipment, is based on operation with two grinding bowls sunk into a disk that achieves extremely high rotational speeds of up to 1100 rpm and centrifugal accelerations of up to 95 times the force of gravity. Main components of the experiments; ball mill, stainless steel bowl / balls and powder are shown in Figure 7.



Figure 7. Fritsch Pulverisette 7 Premium Line High Energy Ball Mill, stainless steel bowl / balls and Ni-B powder mixture

For a new set of experiment; sample amount, number of balls, bowl volume, milling time, cooling time and finally the experiment timesheet are the important specifications to decide. Additionally, during high energy ball milling experiments, to prevent any undesirable incident, it is very important to prevent overheating and excess pressure within the bowls. Therefore, cooling time should be considered while scheduling the experiments.

### **2.3. Experimental Method: Milling Pure Nickel Powders**

In order to investigate the effects of milling parameters such as rotation speed, milling time, ball and bowl material type on properties such as particle size, shape and magnetic properties, milling operation was carried out with high purity Ni powder (99.8% purity - Alfa Aesar) having 48  $\mu\text{m}$  particle size, under controlled Argon atmosphere.

### 2.3.1. Milling Process by High Energy Ball Mill

4.080 grams elemental Ni powders were decided to put in each stainless steel bowl in accordance with the planned amount of Ni-B powder compositions. The decision for the amount of Ni<sub>60</sub>B<sub>40</sub> and Ni<sub>80</sub>B<sub>20</sub> powder compositions and ball diameter will be explained detailed in Section 2.5. Number of balls and diameter were used as the same which is decided for Ni-B compositions.

In order to prevent the oxidation of powders, the bowls were filled with argon gas at a pressure about 1 bar before milling. Rotation speed was determined as 250 rpm. Milling was carried out as cycles of 15 minutes composed of 15 minutes milling, 15 minutes rest and 15 minutes milling in sequence. After each milling cycle, the equipment was left to cool down for about 15 minutes, in order to prevent overheating. The powders were milled for 20 hours in total.

### 2.3.2. Characterization

To be able to observe the changes with milling time, milling process has been interrupted after certain time periods and some sample of powders were taken out of the bowls for characterization after 1, 5, 10 and 20 hours of milling. For characterization; phase analysis, microstructure and morphology, particle size and magnetic properties has been examined. The phase analysis of the ground powders was realized using XRD method. Diffractograms were obtained in a range of  $2\Theta=5-110^\circ$  with Cu-K $\alpha$  radiation at a wavelength of 1.54050 Å using a Rigaku D/Max diffractometer. The microstructure and morphology studies were done using a FEI Nova Nano 430 FEG model scanning electron microscope (FEGSEM). The powders were put on the aluminum sample holder using double-sided adhesive conductive carbon tapes. The crystallite size of the milled powders were calculated from XRD peaks using the Scherrer equation (Equation 1). In the equation  $t$  is the crystallite size,  $\lambda$  is the X ray wavelength,  $\beta$  is the line broadening at half the maximum intensity (FWHM) of the (111) peak, and  $\Theta$  is the Bragg angle.

$$t = \frac{0.9\lambda}{\beta \cos \theta} \quad (\text{Equation 1})$$

In the equation Scherrer constant was taken as 0.9 which is used for spherical particles. Particle size were detected on SEM images, by comparing reference size to the particle sizes on the image. The magnetic properties of the powders were examined using ADE Magnetics EV9 model vibrating sample magnetometer (VSM).

## **2.5. Experimental Method: Milling Nickel-Boron Powders**

### **2.5.1. Milling Process by High Energy Ball Mill**

Milling parameters have been chosen based on the previous studies related to Ni-B mechanical alloying. Corrias et. al (Corrias, Ennas, Marongiu, et al., 1995) indicated that during Ni-B ball milling experiments, when ball diameter scaled down to 4 mm from 8 mm, some intermetallic compounds began to appear in shorter times and the change in rotating speed has not affected the results in a considerable amount. Consequently, they showed that different energetic conditions impacted the rate of the process, but no remarkable effect had been observed either on the reaction path or on the final products.

Two different alloy compositions have been defined as  $\text{Ni}_{80}\text{B}_{20}$  and  $\text{Ni}_{60}\text{B}_{40}$ . Elemental compositions were determined according to the phase diagram of Ni-B which is given in Figure 2 and the reason for choosing these compositions is that these are near the ratios of eutectics and intermetallic compounds occurred. According to the requirements of the planned characterization analyses approximate initial sample amount needed was determined. Then, elemental Nickel and Boron powders were weighed based on calculated amounts for  $\text{Ni}_{80}\text{B}_{20}$  and  $\text{Ni}_{60}\text{B}_{40}$  and put to the bowls. Initial powder materials were Ni powder with 99.8% purity, approximately 48  $\mu\text{m}$  in size and B powder with 98% purity, approximately 44  $\mu\text{m}$  in size.

From the required approximate amount of sample, bowl volume was defined. Milling operation has been carried out with two 20 mL atmosphere-controlled stainless steel bowls and stainless steel balls. Ball amount was determined according to the bowl size as 80 balls (each 5 mm in diameter and 0.51 grams in weight) for each bowl from the given instructures of the milling equipment. Then, powder amount was

calculated based on ball to powder weight ratio which was determined as 10:1. Consequently, 4.080 grams total sample were put in each bowl.

Similar to the pure Ni, in order to prevent oxidation of powders, the bowls were filled with argon gas at a pressure about 1 bar. Milling was carried out as cycles of 15 m at 250 rpm. The powders were milled for 80 h in total.

### **2.5.2. Characterization**

Milling process has been interrupted after 1, 5, 10, 20, 40, 60 and 80 h and samples were taken from each bowls to carry out required analyses for characterization. For this purpose; phase analysis, microstructure and morphology, particle size and magnetic properties have been examined. The same equipments, conditions and methods have been used as in characterization of pure Ni. In addition, for the two compositions, to be able to compare the solid-phase phase transformations and to determine the equilibrium phases in solid-phase achieved by slow cooling rates, thermal analysis have been done using SETARAM, Differential Scanning Calorimetry (DSC), in a range up to 1200 °C with 20 K/min heating rate.

Energy Dispersive Spectroscopy (EDS) analysis which is normally done to obtain elemental percentages of the components observed on SEM, has not been done during this study since Boron has a small atomic number and the radiation of boron atom cannot be obtained in the EDS analysis, so the results of such an analysis would have given wrong results.

## CHAPTER 3

### RESULTS AND DISCUSSIONS

#### 3.1. Milling of Pure Nickel Powders

XRD curves, for initial and milled Nickel powders for different milling times were given in Figure 8. As it is known, Nickel has Face Centered Cubic (FCC) structure and for an FCC lattice, all indices should be either even or odd. The diffraction peaks of Ni were indexed as (111), (200), (220), (311) and (222), respectively.

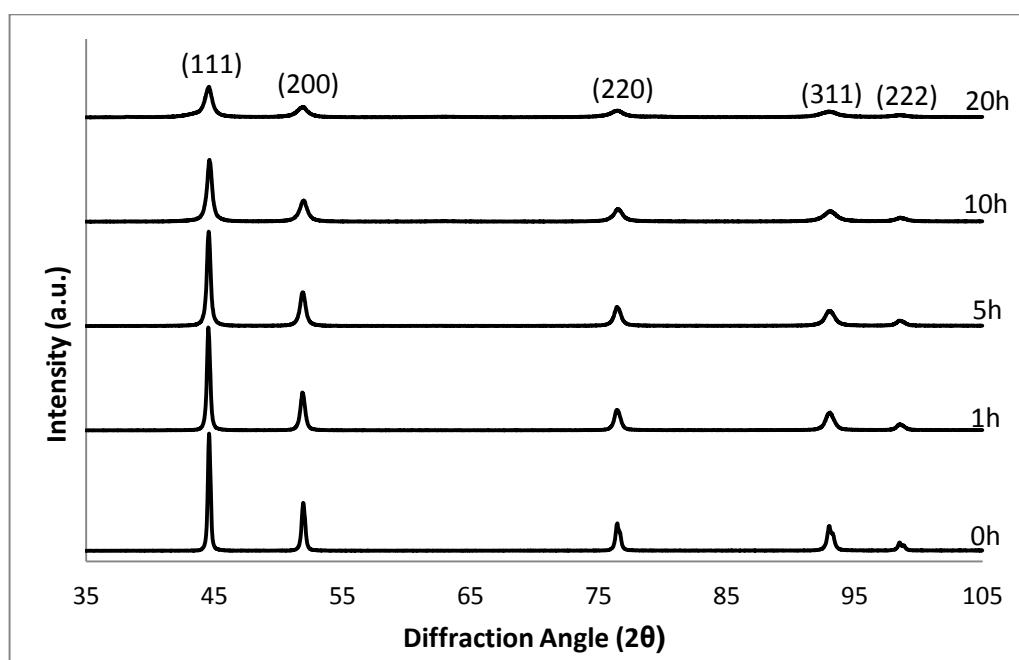


Figure 8. XRD patterns, for initial and milled pure Nickel powders for different time periods

If the diffractograms of the initial powders and powders milled up to 20 h are examined it can be seen that, there is no additional peak of oxide or impurity and no remarkable shifting of the existing peaks towards lower or higher Bragg angles.

Besides, a significant peak broadening, increasing with the milling time, can be observed at a first glance. This is explained with the decrease in crystallite size. Peak broadening can be clearly seen in detail in Figure 9.

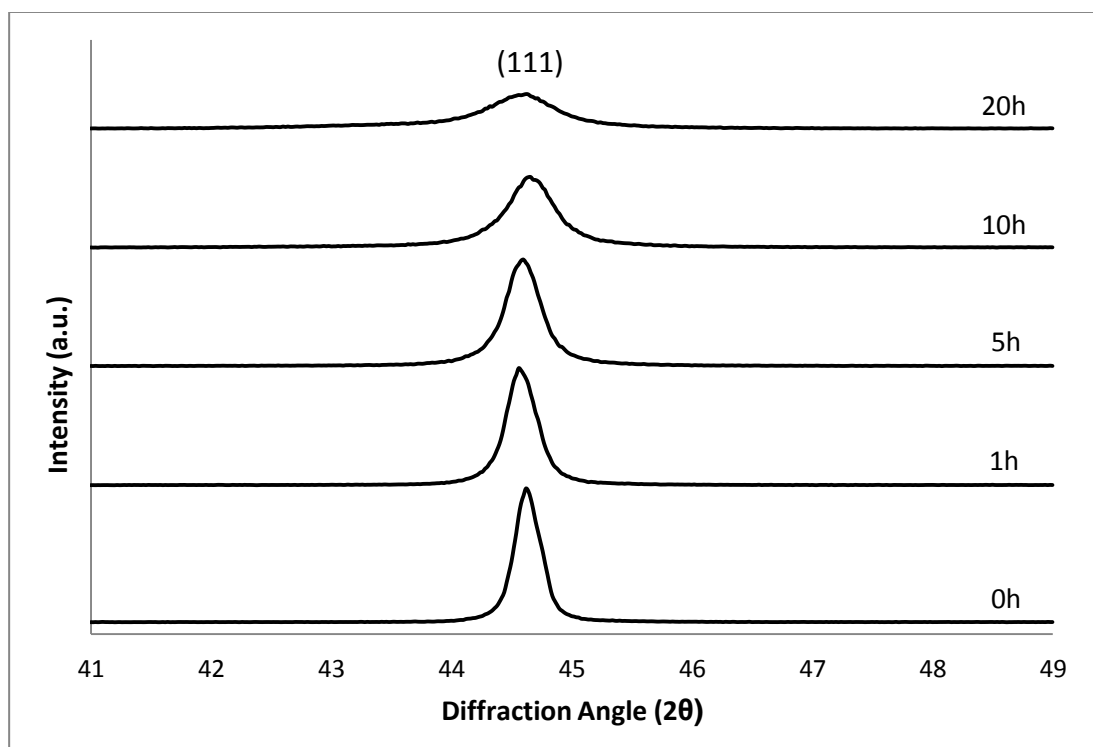


Figure 9. Detailed XRD patterns of initial and milled pure Ni powders for different time periods

By the aid of (111) peak, for pure Ni, crystallite sizes calculated using Scherrer equation were given in Table 2. For these calculations, since the sizes are too small, peak broadening due to instrument has been neglected. In addition, non-uniform distortion contribution to microstrain broadening has been neglected. As it can be seen from the table, as crystallite size of unmilled pure Ni is 33 nm, it decreases to 13 nm, after milling for 20 h.

Table 2. The crystallite sizes, calculated by the Scherrer equation, changing by milling time

Milling Time (h)	Pure Ni Crystallite Size (nm)
0	33
1	29
5	25
10	19
20	13

To observe particle morphology (spherical, cubic, stick, etc.), changes in morphology and size, scanning electron microscopy studies have been carried out. The results of scanning electron microscopy studies can be seen in Figure 10.

SEM analyses showed that there is notable decrease in the particle size with increasing milling time. Examination with high magnification during scanning electron microscopy studies revealed that particle size has been reduced down to 390 nm from 48  $\mu\text{m}$  after 20 h of milling. Besides, it is seen that, the morphology of the initial spherical particles has become deformed with milling operation.

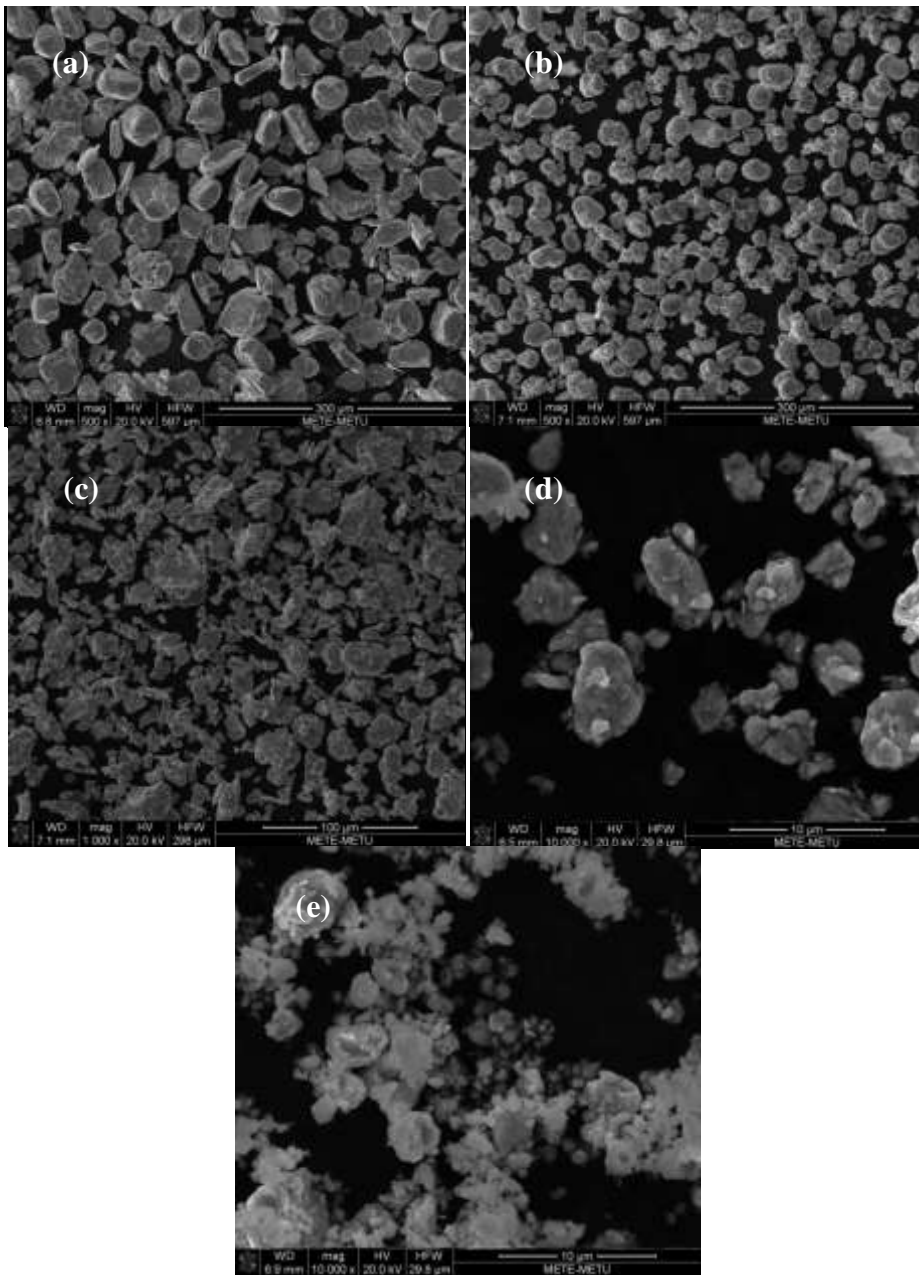


Figure 10. SEM images of (a) unmilled pure Ni powders and powders milled for (b)1 h, (c)5 h, (d)10 h, (e)20 h.

Moreover, how the milling operation affect the magnetic properties of the material has been investigated. Hysteresis curves of unmilled pure Ni and milled pure Ni for different time intervals have been given in Figure 11.

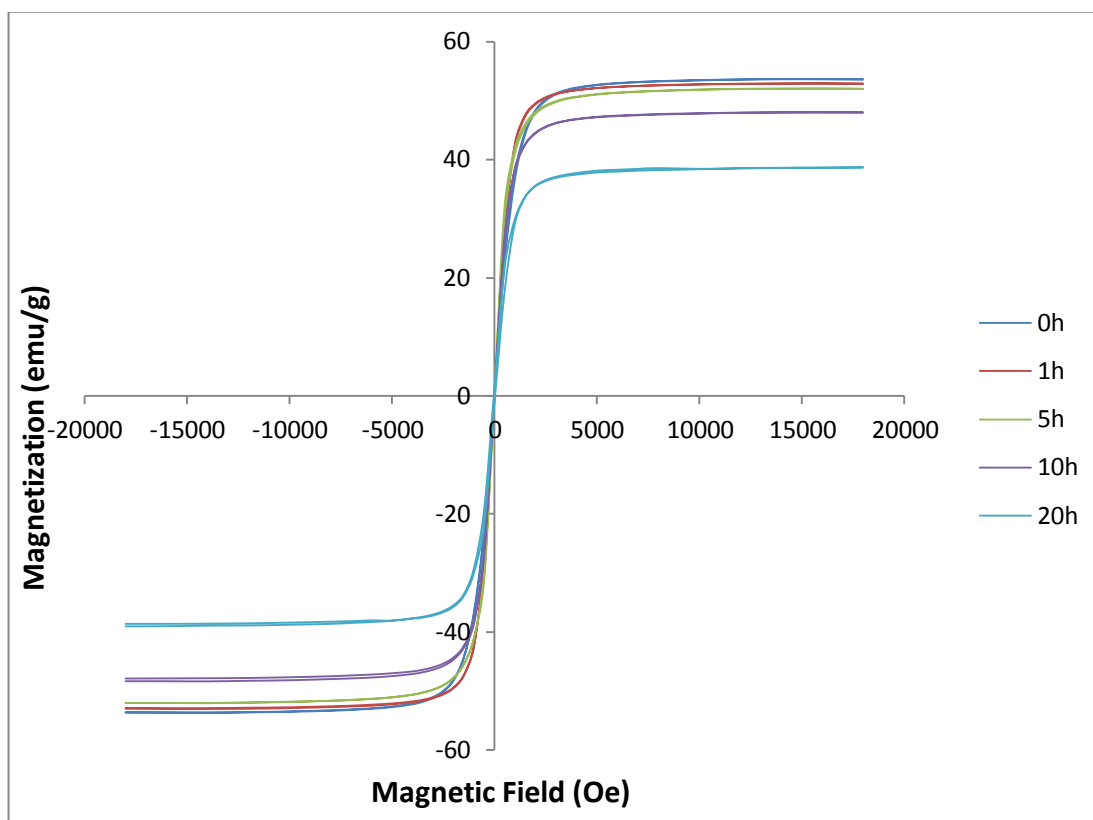


Figure 11. Hysteresis curves of unmilled pure Ni powders and Ni powders milled for 1, 5, 10 and 20 h

Magnetic parameters obtained from the same measurements have been given in the table below.

Table 3. Magnetic parameter values of initial Ni powders and Ni powders milled for 1, 5, 10 and 20 h

Milling time (h)	Saturation Mag., Ms, (emu/g)	Remanent Mag., Mr, (emu/g)	Squareness, S, (Mr/Ms)	Coercivity, Hc, (Oe)
0	53.7	0.1	0.002	2.0
1	53.0	0.3	0.005	4.8
5	52.2	0.4	0.008	6.4
10	48.2	0.1	0.002	2.2
20	38.9	1.3	0.034	33.4

As known, Ni is one of the few ferromagnetic metals. Unmilled and milled for different times, all of the pure Ni powders exhibit soft magnetic behavior. Changes in magnetic properties can be seen in Figure 12. As it is seen from the graph that, powders milled for 0h, 1h and 5h have quite similar magnetic properties. With further increasing the milling time, Ms values decreased and Hc values increased. As the particle size decreases, size of magnetic domains including magnetic moments changes and particles even may form single domains. Hence, there is not any need to provide external energy, applying external field and magnetization decreases.

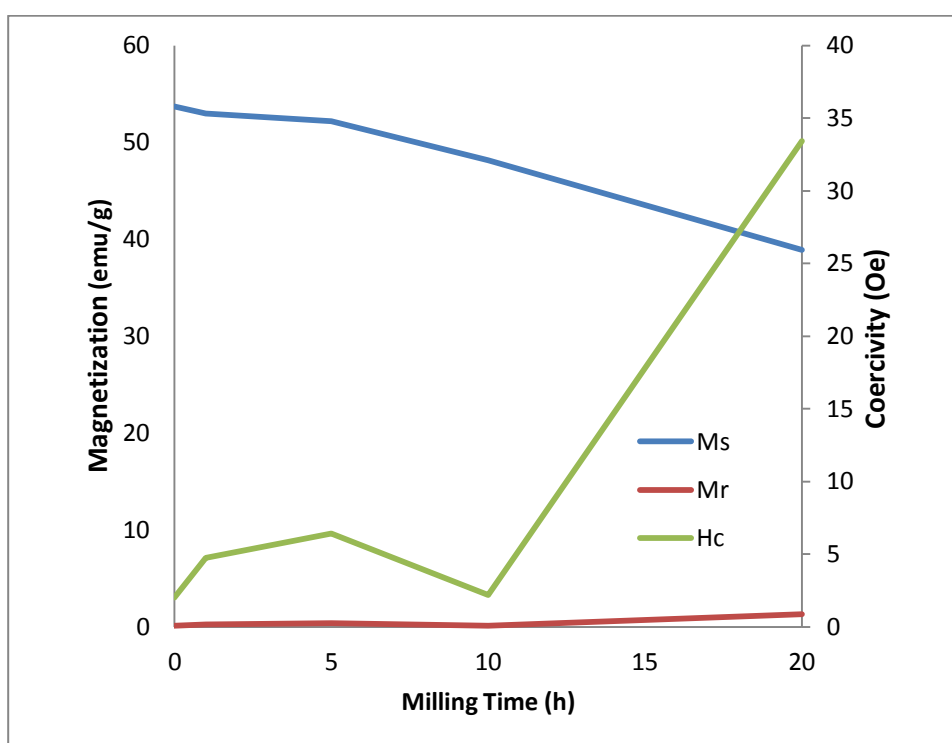


Figure 12. Change in saturation magnetization, remanent magnetization and coercivity against unmilled and milled pure Ni powder for different time intervals

### 3.2. Milling of Nickel Boron Powders

Starting from the initial  $\text{Ni}_{80}\text{B}_{20}$  and  $\text{Ni}_{60}\text{B}_{40}$  composition powders prepared from pure Ni and B powders, milling operation has been carried out up to 80 hours. After certain milling time periods, samples were taken out of the bowls for characterization.

XRD curves of these samples for the whole range and every milling step were given in Figure 13 and Figure 15 for  $\text{Ni}_{80}\text{B}_{20}$  and in  $\text{Ni}_{60}\text{B}_{40}$  compositions respectively.

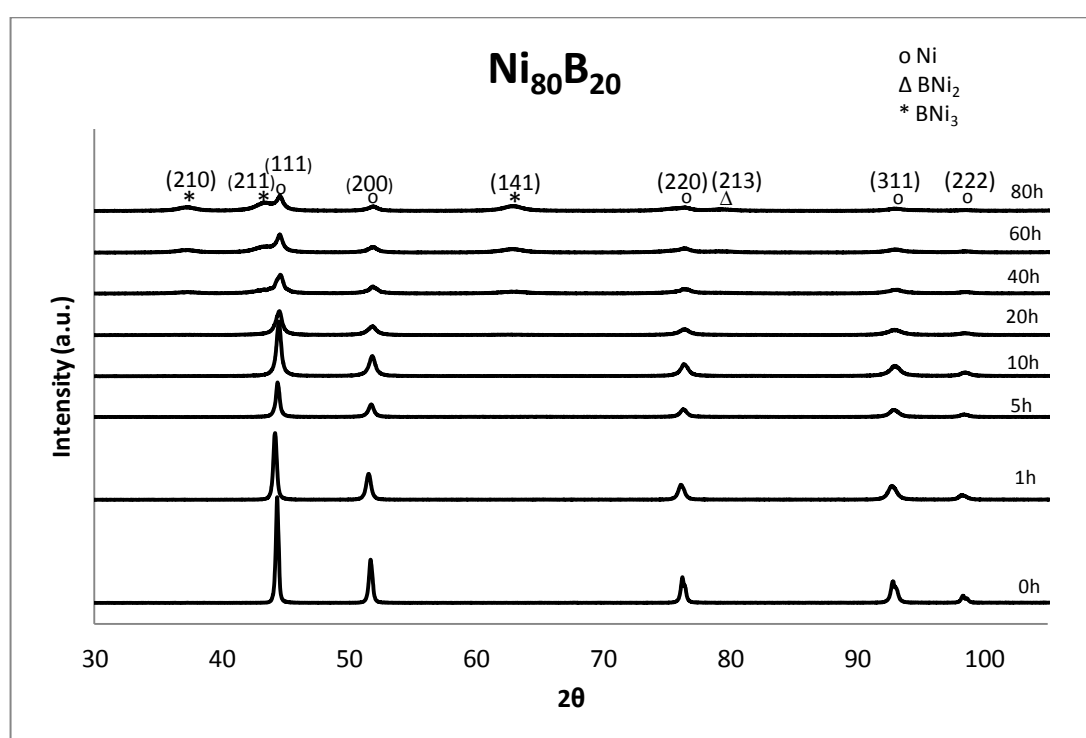


Figure 13. XRD curves of  $\text{Ni}_{80}\text{B}_{20}$ , initial powders and powders ball milled for 1, 5, 10, 20, 40, 60 and 80 h.

For the samples obtained from last three milling steps, XRD curves in detail were given in Figure 14 for  $\text{Ni}_{80}\text{B}_{20}$  composition and in Figure 16 for  $\text{Ni}_{60}\text{B}_{40}$  composition.

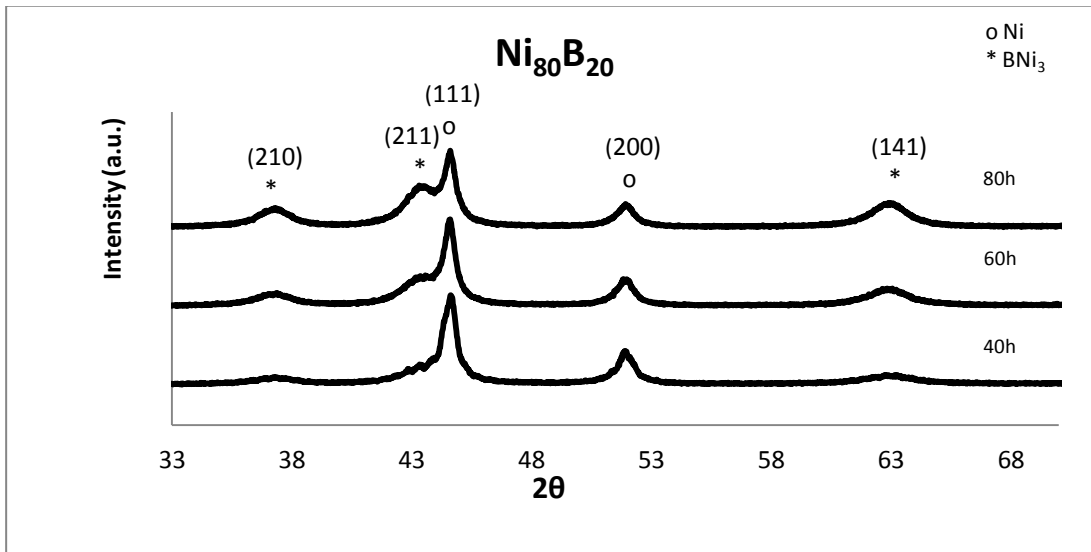


Figure 14. XRD curves of Ni<sub>80</sub>B<sub>20</sub> in detail for milled powder for 40, 60 and 80 h.

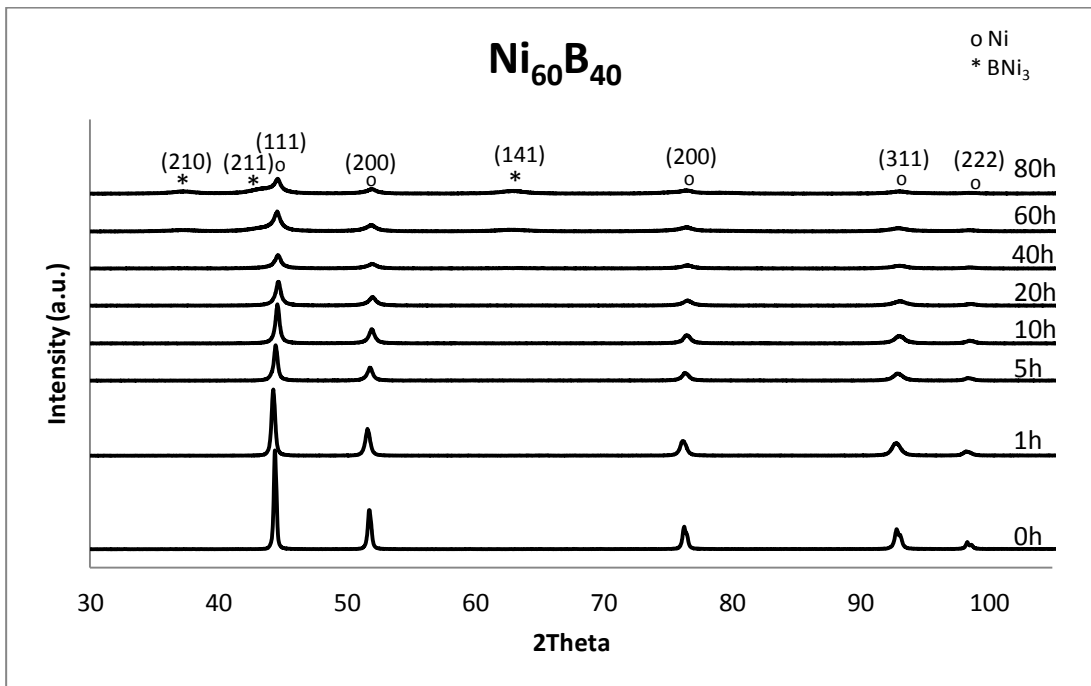


Figure 15. XRD curves of Ni<sub>60</sub>B<sub>40</sub>, initial powders and powders ball milled for 1, 5, 10, 20, 40, 60 and 80 h.

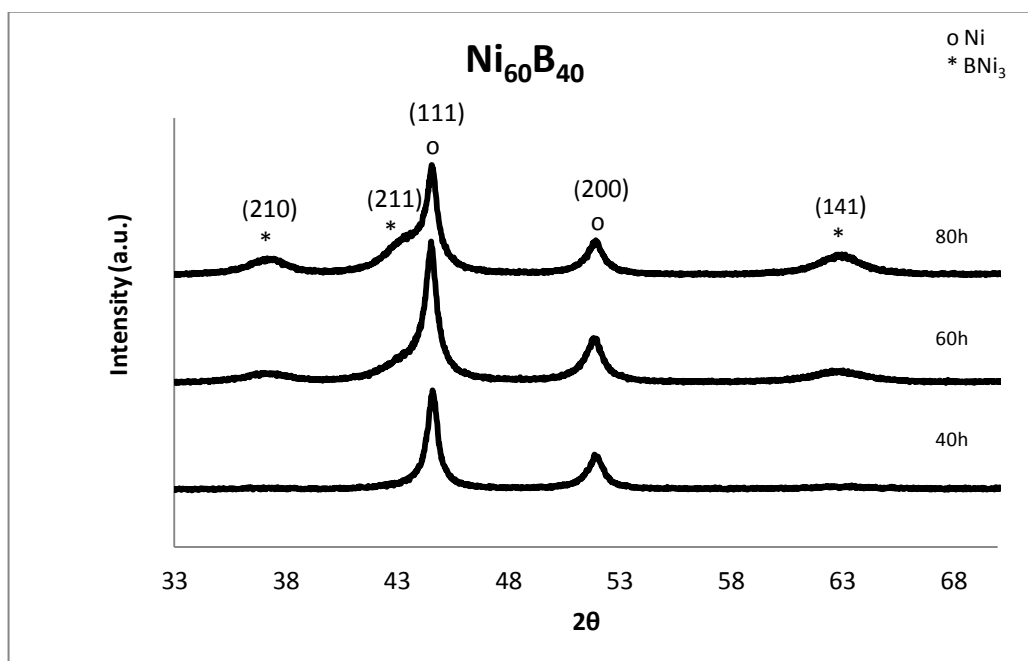


Figure 16. XRD curves of  $\text{Ni}_{60}\text{B}_{40}$  in detail for milled powder for 40, 60 and 80 h

As it can be seen on the phase diagram of Ni-B system, given in Figure 2, at  $\text{Ni}_{80}\text{B}_{20}$  atomic composition, only FCC Nickel and Rhombohedral Boron phases are stable at room temperature. The contribution of Boron is undetectable here as its scattering power is low. Only peaks of Ni being in an amorphous matrix has been clearly detected until intermetallic compounds start to form.

When XRD curves of the two compositions are examined it is seen at the first glance that, peak broadening which means the reduction in crystal size has occurred and increased after every milling operation. Furthermore, intensity of the peaks decreased while milling time increased. (222) Ni peak disappears after 80 hours of milling, for both compositions. Additionally, only a slight shifting, through lower Bragg angles, was observed after one hour of milling for both compositions. This shifting could be explained by the compression of lattice structure after milling operation.

For both compositions there is no remarkable additional peaks until 40 h milling. For  $\text{Ni}_{80}\text{B}_{20}$  composition, formation of  $\text{Ni}_3\text{B}$  intermetallic eutectic structure phase can be observed notably after 40 hours of milling. It is understood from the increase in the intensity of  $\text{Ni}_3\text{B}$  peaks that, the amount of this phase increased when the milling time increased to 60 h and 80 h. The structure of  $\text{Ni}_3\text{B}$  intermetallic phase is

Orthorombic and its type is  $CFe_3$  (Villars, 1998). For  $Ni_{60}B_{40}$  composition, formation of  $Ni_3B$  intermetallic phase is observed notably after 60 hours of milling. In addition, for  $Ni_{80}B_{20}$  composition,  $Ni_2B$  intermetallic compound starts to form after 40 hours of milling, whereas there is no such a formation for  $Ni_{60}B_{40}$ .

By use of XRD diffraction patterns, the crystallite sizes that were calculated by Scherrer Equation are given in Table 4. From the Table it is clearly seen that crystallite size decreases while milling time increases, as expected. Finally, after 80 hours of milling it shrinks to approximately 9 nm in both samples.

Table 4. The crystallite sizes, calculated by the Scherrer equation, changing by milling time

Milling Time (h)	$Ni_{60}B_{40}$ Crystallite Size (nm)	$Ni_{80}B_{20}$ Crystallite Size (nm)
0	35	32
1	27	27
5	26	25
10	23	20
20	19	15
40	12	11
60	10	9
80	9	8

To investigate the particle morphology (cubic, spherical, plate like, etc.) and particle size, scanning electron microscopy (SEM) analysis have been done. As a result of SEM analysis, obtained microstructural images of initial and milled  $Ni_{80}B_{20}$  powders are given in Figure 17.

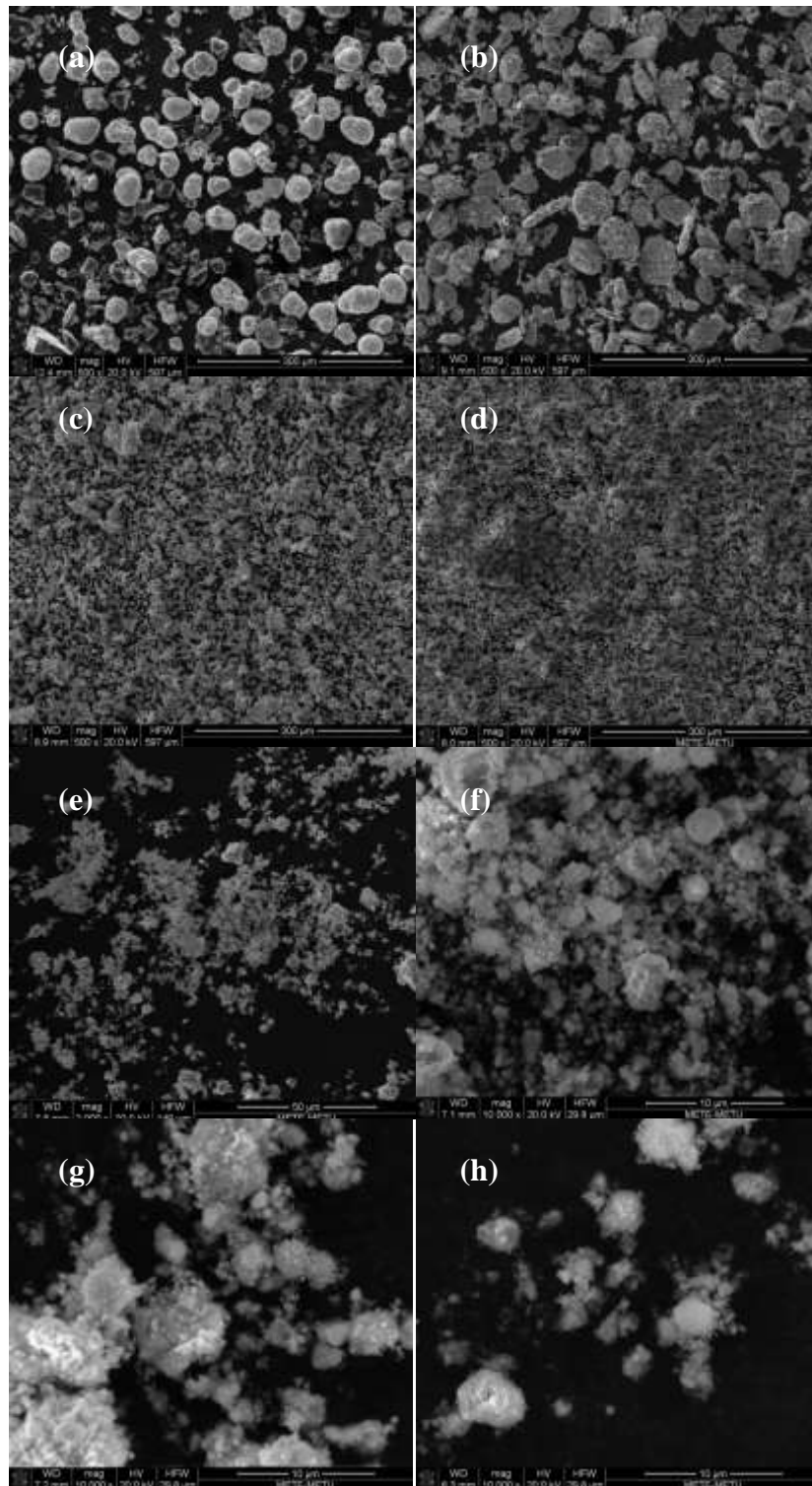


Figure 17. SEM images for  $\text{Ni}_{80}\text{B}_{20}$  composition powder milled for (a) 0 h (initial), (b) 1 h, (c) 5 h, (d) 10 h, (e) 20 h, (f) 40 h, (g) 60 h, (h) 80 h.

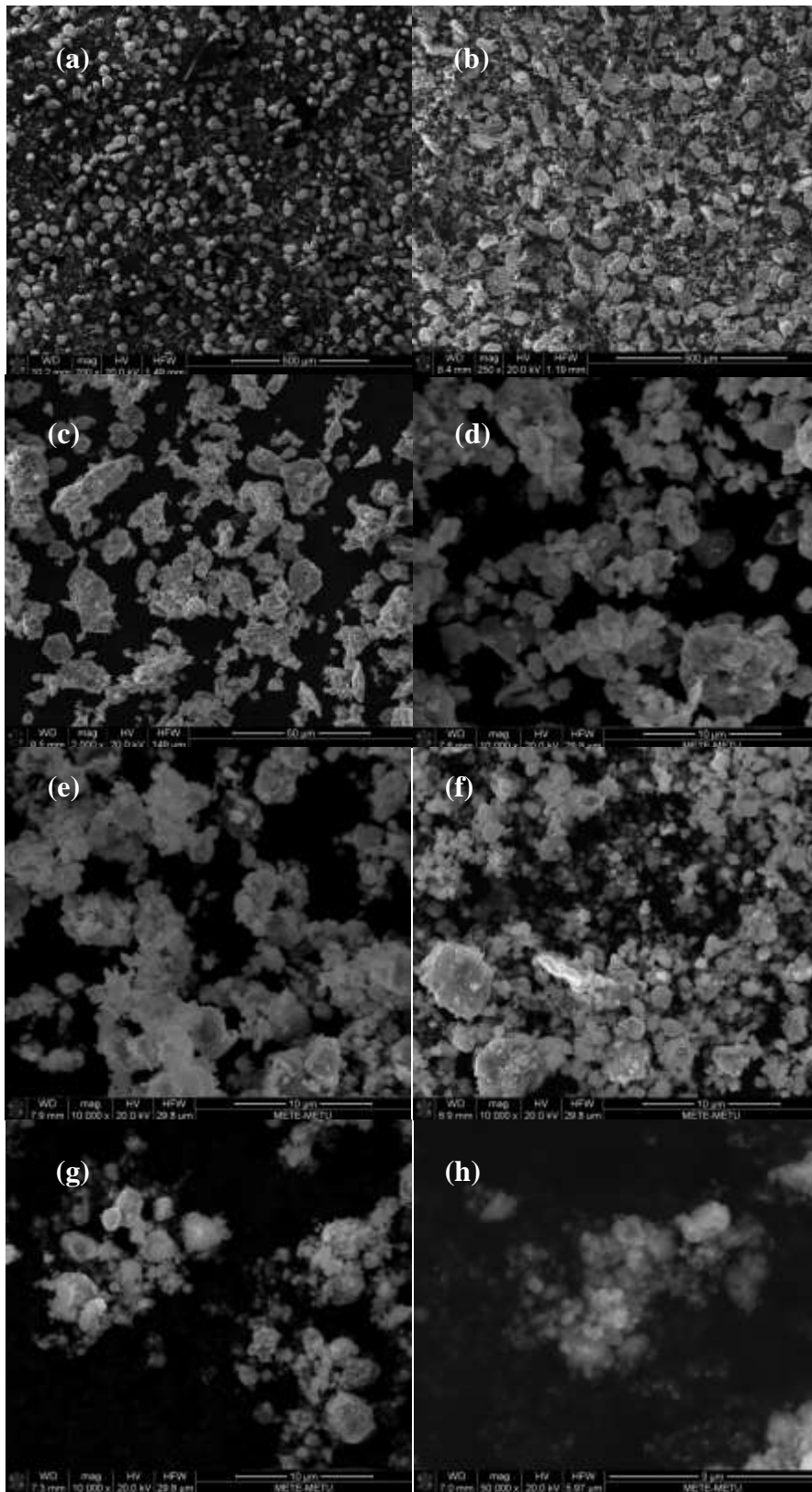


Figure 18. SEM images for  $\text{Ni}_{60}\text{B}_{40}$  composition powder milled for (a) 0 h (initial), (b) 1 h, (c) 5 h, (d) 10 h, (e) 20 h, (f) 40 h, (g) 60 h, (h) 80 h.

When SEM images were examined in terms of morphologies of the particles, for the initial powder, it was seen that the spherical particles are Ni where the plate like ones are Boron. SEM images also showed that as milling time increases, particle size decreases and definite shapes of the particles become deformed. High magnification SEM measurements for both composition samples of the last two step of milling operations are given in Figure 19 and Figure 20.

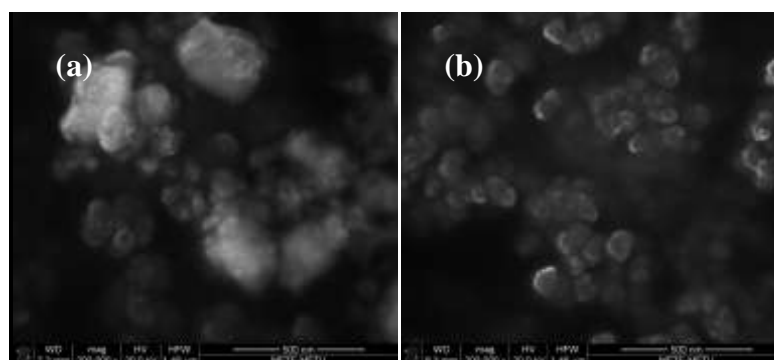


Figure 19. High Resolution SEM images for Ni<sub>80</sub>B<sub>20</sub> composition powder milled for (a) 60 h (b) 80 h

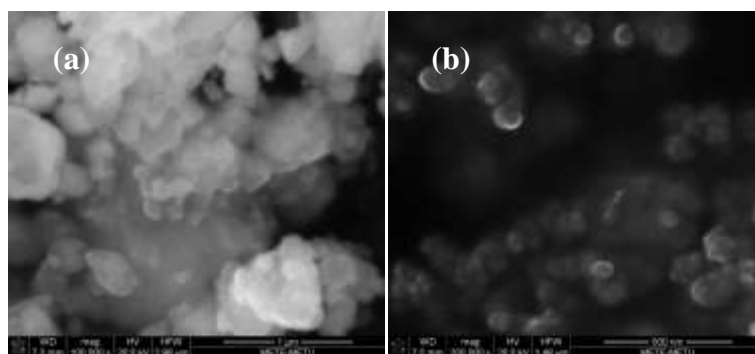


Figure 20. High Resolution SEM images for Ni<sub>60</sub>B<sub>40</sub> composition powder milled for (a) 60 h (b) 80 h

Being similar to the milling of pure Ni, there is significant decrease in the particle size with increasing milling time, as expected. Examination with high magnification during scanning electron microscopy studies and measurements revealed that after 80 hours of milling, particle size ranges between 20 nm to 110 nm for samples of both compositions.

Although a particle size range is defined for both samples by the aid of high magnification SEM measurements, as these particles show magnetic behavior, the definition of images was not high enough for bigger magnifications. Hence, it is not certain whether there are particles smaller than 20 nm or not.

Thermal analyses were done in order to confirm the formation of amorphous phases. DSC thermograph belonging to both compositions that can be seen in Figure 21 and 22 show characteristic features of a DSC curve corresponding to glass transition, crystallization and melting respectively. Due to crystallization from the amorphous phase can be seen.

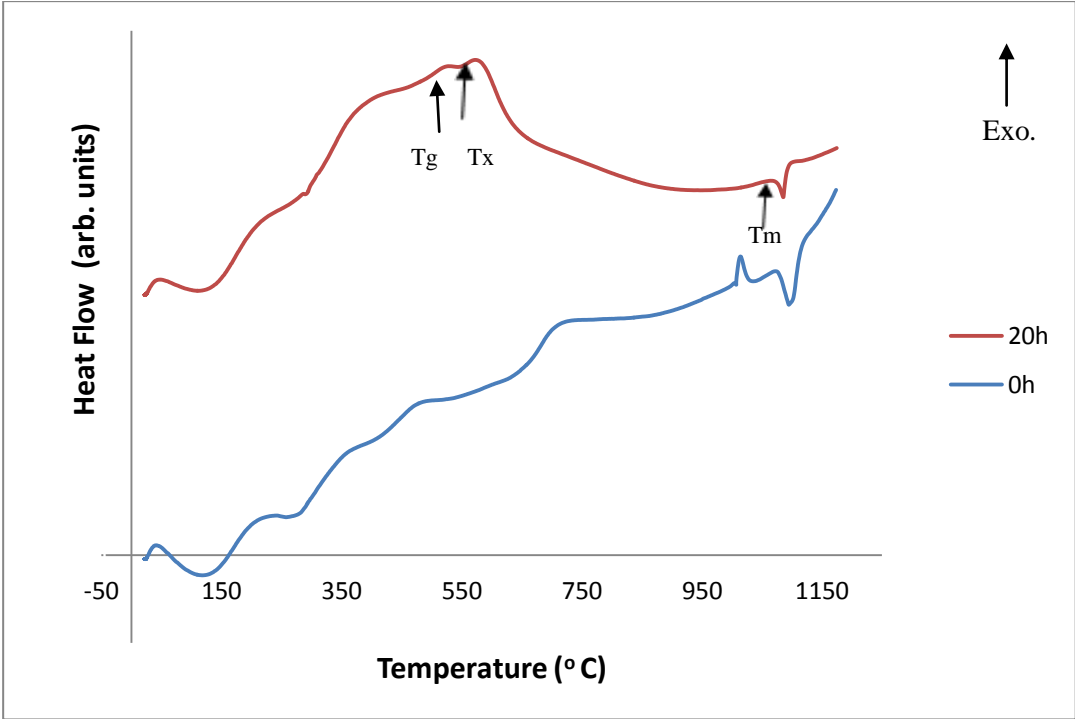


Figure 21. DSC analyses of the initial and milled powder for 20 h for Ni<sub>80</sub>B<sub>20</sub> sample

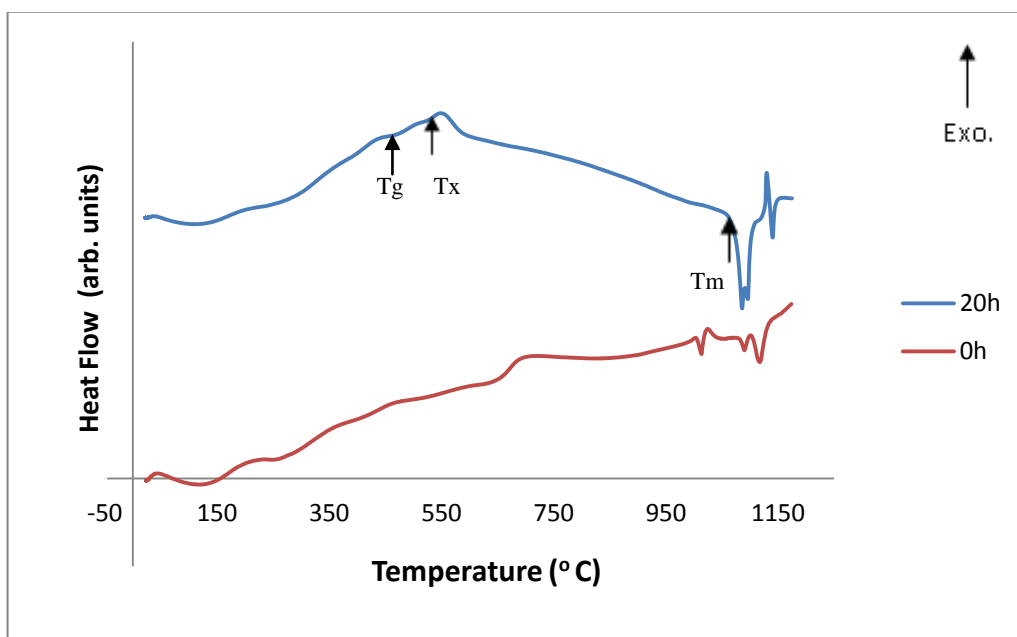


Figure 22. DSC analyses of the initial and milled powder for 20 h for  $\text{Ni}_{60}\text{B}_{40}$  sample

Magnetic properties of the samples has been investigated for powders milled for different time periods. Hysteresis curves obtained for this purpose given in the Figure 23 for  $\text{Ni}_{80}\text{B}_{20}$ .

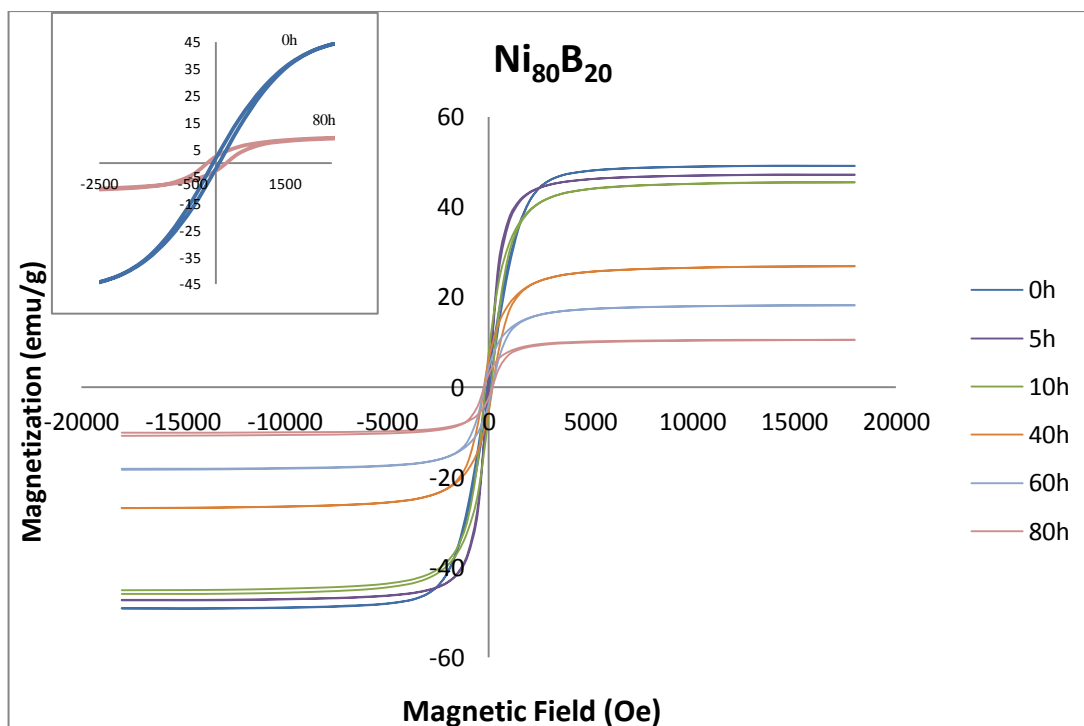


Figure 23. Hysteresis curves for initial  $\text{Ni}_{80}\text{B}_{20}$  powder and powders milled for different time periods.

In Figure 23 inset shows the detailed part of hysteresis belonging to powders milled for 0 h and 80 h.

Parameters measured to show magnetic properties of unmilled and milled Ni<sub>80</sub>B<sub>20</sub> and Ni<sub>60</sub>B<sub>40</sub> powders are given in Table 5 and Table 6 respectively.

Table 5. Magnetic properties of initial Ni<sub>80</sub>B<sub>20</sub> powder and powders milled for different time periods.

Milling time (h)	Saturation Mag., Ms, (emu/g)	Remanent Mag., Mr, (emu/g)	Squareness, S, (Mr/Ms)	Coercivity, Hc, (Oe)
0	49.1	2.0	0.040	63.3
1	51.1	0.02	0.000	0.5
5	47.2	0.1	0.002	1.8
10	45.7	6.8	0.149	149.2
20	35.3	2.3	0.065	77.8
40	26.9	5.7	0.211	207.9
60	18.3	4.1	0.224	199.5
80	10.7	2.7	0.250	201.0

Phases within the initial structures are only Ni which is a ferromagnetic material showing magnetic properties and B which does not show magnetic behaviour. As it can be seen from Table 5 and Table 6, saturation magnetization values shows a general decrease with the increasing milling time whereas coercivity values increases generally. Initially, both compositions and pure Ni displays similar magnetic properties; however they differentiate with further milling. Intermetallic phases formed at the last steps of milling also considered as a parameter that affects magnetic properties. Since particle sizes for both compositions are similar, volume fraction of magnetic phases is the dominant factor for saturation magnetization values.

The same studies were realized to find out magnetic properties of the Ni<sub>60</sub>B<sub>40</sub> sample. Hysteresis curves for Ni<sub>60</sub>B<sub>40</sub> are given in Figure 24. In the figure inset shows the detailed part of hysteresis belonging to powders milled for 0 h and 80 h.

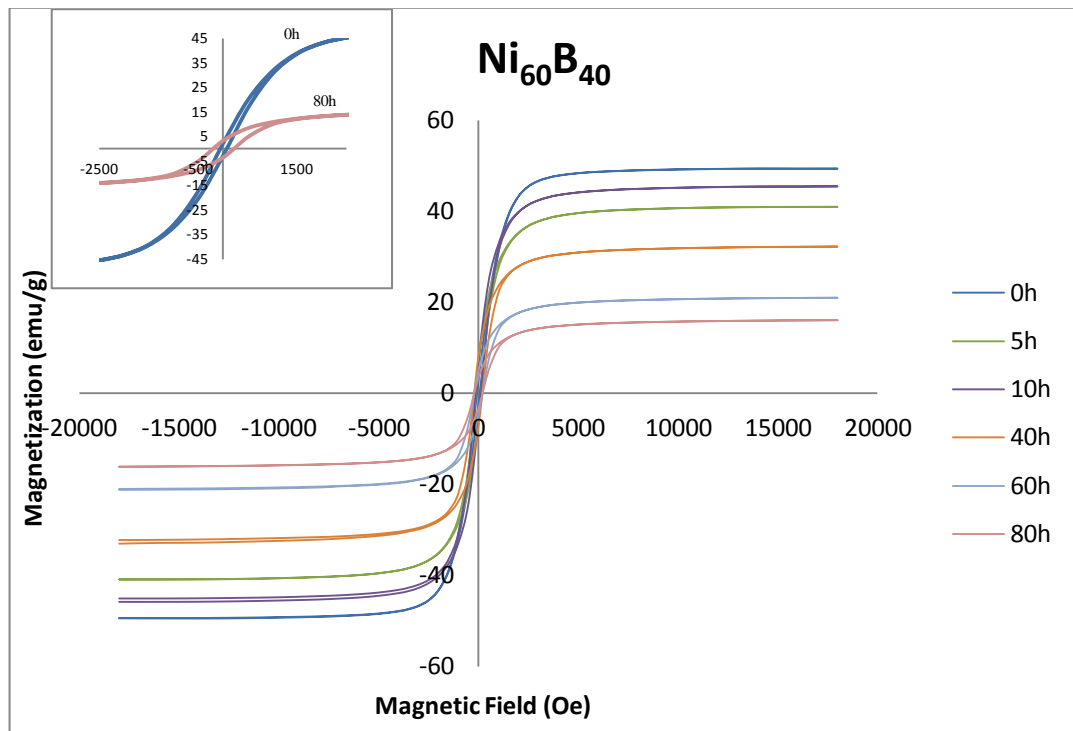


Figure 24. Hysteresis curves for initial  $\text{Ni}_{60}\text{B}_{40}$  powder and powders milled for different time periods

For both composition, with increasing milling time, the area of the hysteresis increases. The area of hysteresis loop is related to the amount of energy dissipation upon reversal of the field and a narrow hysteresis loop indicates a small amount of energy dissipation which is desirable for transformer and motor cores.

Table 6. Magnetic properties of initial  $\text{Ni}_{60}\text{B}_{40}$  powder and powders milled for different time periods.

Milling time (h)	Saturation Mag., Ms, (emu/g)	Remanent Mag., Mr, (emu/g)	Squareness, S, (Mr/Ms)	Coercivity, Hc, (Oe)
0	49.5	2.5	0.051	65.4
1	48.8	0.2	0.003	3.3
5	41.0	6.2	0.152	136.2
10	45.7	6.5	0.143	136.1
20	26.2	3.0	0.112	81.5
40	32.6	7.7	0.235	201.2
60	21.1	4.8	0.229	203.9
80	16.2	3.5	0.210	207.3



## CHAPTER 4

### CONCLUSION

In this study, ball milling which is a type of mechanical alloying has been performed aiming to produce nanocrystalline/amorphous, alloy/intermetallic phases in Ni-B system. Two different compositions ( $\text{Ni}_{80}\text{B}_{20}$  and  $\text{Ni}_{60}\text{B}_{40}$ ) of elemental Ni and B powders were prepared for separate bowls. They have been milled for 1, 5, 10, 20, 40, 60 and 80 hours and samples were taken from the bowls at every milling step for characterization. Magnetic measurements, XRD analyses, thermal analysis and SEM studies have been carried out for characterization studies.

For both compositions, peak broadening in the X-Ray diffractograms and calculations based on Scherrer Equation have shown that, crystal size decreased after every milling step, as expected. Along with peak broadening in XRD curves, DSC analyses pointed out to amorphous structure. According to SEM analyses, with increasing milling time, average particle size decreased and number of sub-micron particles increased in both mixtures. The size of the sub-micron particles have been observed in a range between 20 nm to 110 nm.

For both compositions there is no remarkable additional peaks until 40 h milling. For  $\text{Ni}_{80}\text{B}_{20}$  composition, formation of  $\text{Ni}_3\text{B}$  intermetallic eutectic structure phase can be observed notably after 40 hours of milling. It is understood from the increase in the intensity of  $\text{Ni}_3\text{B}$  peaks that, the amount of this phase increased when the milling time increased to 60 h and 80 h. For  $\text{Ni}_{60}\text{B}_{40}$  composition, formation of  $\text{Ni}_3\text{B}$  intermetallic phase is observed notably after 60 hours of milling. In addition, for  $\text{Ni}_{80}\text{B}_{20}$  composition,  $\text{Ni}_2\text{B}$  intermetallic compound formation is observed after 40 hours of milling.

The main motivation to investigate nanoscale magnetic materials is the notable change of magnetic properties of these systems. In this study, magnetic measurements indicated to a general decrease in saturation magnetization and increase in coercivity. For both samples, hysteresis increased with milling. Consequently, with the increasing milling time, ferromagnetism became more effective.

For further research, process parameters (rotating speed, cycle intervals, bowl and ball type and size etc.) can be changed. Longer milling times might be performed. Different compositions can be determined on the basis of phase diagram and milled for alloying and intermetallic phases to occur. Theoretical studies can be carried out based on Ni-B binary system and experimental results also can be compared to the theoretical results. Furthermore, for imaging and better prediction of particle size distribution Transition Electron Microscopy (TEM) analysis with special apparatus can be utilized.

## REFERENCES

- Angelo, P. G., & Subramaian, R. (2008). Powder Metallurgy: Science, Technology and Applications.
- Belloni, J., Mostafavi, M., Remita, H., Marignier, J.-L., & Delcourt, and M.-O. (1998). Radiation-induced synthesis of mono- and multi-metallic clusters and nanocolloids. *New Journal of Chemistry*, 22(11), 1239–1255. doi:10.1039/a801445k
- Brandon, D., & Kaplan, W. D. (2013). Microstructural Characterization of Materials. John Wiley & Sons.
- Campbell, A. N., Barbour, J. C., Hills, C. R., & Nastasi, M. (1989). The formation of amorphous Ni–B by solid state and ion-beam reaction. *Journal of Materials Research*, 1303–1306. doi:10.1557/JMR.1989.1303
- Chen, C. ;, Bai, Y., Chen, W., & Xuchu, Y. (2013). Boron influence on structures and properties in Nickel-Based Alloys.
- Chen, Y., & Chen, Y. (1994). Hydrogenation of pamchloronitrobenzene nickel borides, *115*(94), 45–57.
- Chen, Y., Liaw, B., & Chiang, S. (2005). Selective hydrogenation of citral over amorphous NiB and CoB nano-catalysts, *284*, 97–104. doi:10.1016/j.apcata.2005.01.023
- Chiang, S., Liaw, B., & Chen, Y. (2007). Preparation of NiB nanoparticles in water-in-oil microemulsions and their catalysis during hydrogenation of carbonyl and olefinic groups, *319*, 144–152. doi:10.1016/j.apcata.2006.11.028
- Corrias, A., Ennas, G., Marongiu, G., Musinu, A., Paschina, G., & Zedda, D. (1995). The synthesis of nanocrystalline nickel boride powders by ball milling of elemental components. *Materials Science and Engineering: A*, 204(1-2), 211–216. doi:10.1016/0921-5093(95)09963-8
- Corrias, A., Ennas, G., Musinu, A., Paschina, G., & Zedda, D. (1995). The preparation of nanocrystalline boride powders via a solid state reaction induced by the ball milling of nickel-boron mixtures, *193*, 565–569.
- Davis, J. R. (2000a). *Nickel, Cobalt and Their Alloys* (1st ed.). ASM International, The Materials Information Society.

- Davis, J. R. (2000b). *Nickel, Cobalt and Their Alloys* (1st ed.). ASM International, The Materials Information Society.
- Davis, J. R. (2000c). *Nickel, Cobalt and Their Alloys* (1st ed.). ASM International, The Materials Information Society.
- Davis, J. R. (2000d). *Nickel, Cobalt and Their Alloys* (1st ed.). ASM International, The Materials Information Society.
- Destrée, C., & Nagy, J. B. (2006). Mechanism of formation of inorganic and organic nanoparticles from microemulsions, *126*, 353–367. doi:10.1016/j.cis.2006.05.022
- Diabb, J., Juárez-Hernandez, a., Colas, R., Castillo, a. G., García-Sanchez, E., & Hernandez-Rodriguez, M. a. L. (2009). Boron influence on wear resistance in nickel-based alloys. *Wear*, *267*(1-4), 550–555. doi:10.1016/j.wear.2008.12.046
- Eastman, J. A., & Weertman, J. R. (1997). Elastic And Tensile Behavior Of Nanocrystalline Copper And Palladium, *45*(10).
- Erb, U. (1995). Electrodeposited Nanocrystals : Synthesis , Properties And Industrial Applications, *6*, 533–538.
- Fadaie, A., Mekhrabov, A. O., & Akdeniz, M. V. (2014). Synthesis and Characterization of Fe<sub>80</sub>B<sub>20</sub> Nanoalloys Produced by Surfactant Assisted Ball Milling, *125*(2), 597–599. doi:10.12693/APhysPolA.125.597
- Ferrando, R., Jellinek, J., & Johnston, R. L. (2008). Nanoalloys: From Theory to Applications of Alloy Clusters and Nanoparticles. *Chemical Reviews*, *108*(3), 846–904. doi:10.1021/cr040090g
- Frey, N. a., & Sun, S. (2009). Magnetic Nanoparticle for Information Storage Applications. *Inorganic Nanoparticles: Synthesis, Applications, and Perspectives*, (Richter), 33–68.
- Geng, J., Jefferson, D. a., & Johnson, B. F. G. (2007). The unusual nanostructure of nickel-boron catalyst. *Chemical Communications (Cambridge, England)*, (9), 969–971. doi:10.1039/b615529d
- Glass, J. a., Kher, S., Kim, Y.-G., Dowben, P. a., & Spencer, J. T. (1990). The Deposition of Nickel Boride Thin Films by Borane and Metallaborane Cluster Compounds. *MRS Proceedings*, *204*. doi:10.1557/PROC-204-439
- Inoue, A., Akihiro, K., & Tsuyoshi, M. (1979). Ni-B and Co-B Amorphous Alloys with High Boron Concentration.
- J. Legrand , A.Taleb, S. Gota , M.J. Guittet, and C. P. (2002). Synthesis and XPS Characterization of Nickel Boride Nanoparticles.

- Jellinek, J. (2008). Nanoalloys: tuning properties and characteristics through size and composition. *Faraday Discussions*, 138, 11–35; discussion 119–135, 433–434. doi:10.1039/b800086g
- Joardar, J., Pabi, S. K., & Murty, B. S. (2007). Milling criteria for the synthesis of nanocrystalline NiAl by mechanical alloying, 429, 204–210. doi:10.1016/j.jallcom.2006.04.045
- Kamel, M. M., Anwer, Z. M., Abdel-Salam, I. T., & Ibrahim, I. S. (2014). Electrodeposition of nanocrystalline Ni-Cu alloy from environmentally friendly lactate bath. *Surface and Interface Analysis*, 46(7), 442–448. doi:10.1002/sia.5525
- Koch, C. C. (1997). Synthesis Of Nanostructured Materials By Mechanical Milling : Problems And Opportunities, 9, 13–22.
- Kumar, K. S., Van Swygenhoven, H., & Suresh, S. (2003). Mechanical behavior of nanocrystalline metals and alloys. *Acta Materialia*, 51(19), 5743–5774. doi:10.1016/j.actamat.2003.08.032
- Leung, K. T. (2013). Sensor Performance and Selectivity by Nanoalloying.
- Li, H., Ding, F., Wang, G., Zhang, J., & Bian, X. (2001). Evolution of small nickel cluster during solidi ® cation, 120, 41–46.
- Li, H., Li, H., Dai, W., & Qiao, M. (2003). Preparation of the Ni-B amorphous alloys with variable boron content and its correlation to the hydrogenation activity, 238, 119–130.
- Li, H., Li, H., Dai, W., Wang, W., & Fang, Z. (1999). XPS studies on surface electronic characteristics of Ni – B and Ni – P amorphous alloy and its correlation to their catalytic properties, 25–34.
- Lü, L., & Lai, M. O. (2013). Mechanical Alloying.
- Mariscal, M. M., Oldani, N. a, Dassie, S. a, & Leiva, E. P. M. (2008). Atomistic computer simulations on the generation of bimetallic nanoparticles. *Faraday Discussions*, 138, 89–104; discussion 119–135, 433–434. doi:10.1039/b706149h
- Massicot, F., Schneider, R., Fort, Y., Illy-Cherrey, S., & Tillement, O. (2000). Synergistic Effect in Bimetallic Ni–Al Clusters. Application to Efficient Catalytic Reductive Dehalogenation of Polychlorinated Arenes. *Tetrahedron*, 56(27), 4765–4768. doi:10.1016/S0040-4020(00)00383-5
- McNamara, K., & Tofail, S. a M. (2013). *10 - Biomedical applications of nanoalloys. Nanoalloys*. Elsevier Inc. doi:http://dx.doi.org/10.1016/B978-0-12-394401-6.00010-2

- Mejía-Rosales, S., Ponce, A., & José-Yacamán, M. (2013). *Experimental techniques for structural characterization. Nanoalloys*. Elsevier Inc. doi:10.1016/B978-0-12-394401-6.00004-7
- Murty, B. S. (1992). Solid state amorphization in binary Ti-Ni, Ti-Cu and ternary Ti-Ni-Cu system by mechanical alloying, *149*, 231–240.
- Murty, B. S., & Rao, M. M. (1995). Milling Maps And Amorphization Mechanical Alloying, *7151(94)*, 2443–2450.
- Nunomura, N., Hori, H., Teranishi, T., Miyake, M., & Yamada, S. (1998). Magnetic properties of nanoparticles in PdNi alloys. *Physics Letters A*, *249(5-6)*, 524–530. doi:10.1016/S0375-9601(98)00779-8
- Pabi, S. K., Joardar, J., Manna, I., & Murty, B. S. (1997). Nanocrystalline phases in Cu-Ni, Cu-Zn and Ni-Al systems by mechanical alloying. *Nanostructured Materials*, *9(1-8)*, 149–152. doi:10.1016/S0965-9773(97)00040-8
- Peng, Z., & Yang, H. (2008). Ag-Pt alloy nanoparticles with the compositions in the miscibility gap. *Journal of Solid State Chemistry*, *181(7)*, 1546–1551. doi:10.1016/j.jssc.2008.03.013
- Portales, H., Saviot, L., Duval, E., Gaudry, M., Cottancin, E., Pellarin, M., ... Broyer, M. (2002). Resonant Raman Scattering by quadrupolar vibrations of Ni-Ag Core-shell Nanoparticles, *65*, 1–5. doi:10.1103/PhysRevB.65.165422
- Raja, R., Golovko, V. B., Thomas, J. M., Berenguer-Murcia, A., Zhou, W., Xie, S., & Johnson, B. F. G. (2005). Highly efficient catalysts for the hydrogenation of nitro-substituted aromatics. *Chemical Communications (Cambridge, England)*, (15), 2026–2028. doi:10.1039/b418273a
- Reddy, B., Nayak, S., Khanna, S., Rao, B., & Jena, P. (1999). Electronic structure and magnetism of Rh<sub>n</sub> (n=2–13) clusters. *Physical Review B*, *59(7)*, 5214–5222. doi:10.1103/PhysRevB.59.5214
- Schaak, R. E., Sra, A. K., Leonard, B. M., Cable, R. E., Bauer, J. C., Han, Y. F., ... Funck, E. S. (2005). Metallurgy in a beaker: Nanoparticle toolkit for the rapid low-temperature solution synthesis of functional multimetallic solid-state materials. *Journal of the American Chemical Society*, *127(10)*, 3506–3515. doi:10.1021/ja043335f
- Schärtl, W. (2010). Current directions in core-shell nanoparticle design. *Nanoscale*, *2(6)*, 829–843. doi:10.1039/c0nr00028k
- Schwartz. (2002). Encyclopedia of materials, parts and finishes. *Materials & Design*. doi:10.1016/0261-3069(93)90020-V

- Sondón, T., Guevara, J., & Saúl, A. (2007). Study of the structure, segregation, and magnetic properties of Ni-Rh clusters. *Physical Review B - Condensed Matter and Materials Physics*, 75(10), 1–10. doi:10.1103/PhysRevB.75.104426
- Suryanarayana, C. (2008). Recent Developments In Mechanical Alloying, 18.
- Taskinen, & Teppo. (1993). Thermodynamic Assessment of NiB Phase Diagram, *Materials Science and Technology*
- Toda, T. (1999). Enhancement of the Electroreduction of Oxygen on Pt Alloys with Fe, Ni, and Co. *Journal of The Electrochemical Society*, 146(10), 3750. doi:10.1149/1.1392544
- Valiev, R. Z., & Alexandrov, I. V. (2002). Paradox of strength and ductility in metals processed by severe plastic deformation, 5–8.
- Villars, P. (1998). Pearson's Handbook Crystallographic Data For Intermetallic Phases.
- Wang, B., Li, B., Zhao, B., & Li, C. Y. (2008). Amphiphilic Janus gold nanoparticles via combining “solid-state grafting-to” and “grafting-from” methods. *Journal of the American Chemical Society*, 130(35), 11594–11595. doi:10.1021/ja804192e
- Wang, Y., Guo, C. X., Wang, X., Guan, C., Yang, H., Wang, K., & Li, C. M. (2011). Hydrogen storage in a Ni–B nanoalloy-doped three-dimensional graphene material. *Energy & Environmental Science*, 4, 195. doi:10.1039/c0ee00357c
- Wang, Y., Liu, J., Wang, K., Chen, T., Tan, X., & Li, C. M. (2011). Hydrogen storage in Ni-B nanoalloy-doped 2D graphene. *International Journal of Hydrogen Energy*, 36(20), 12950–12954. doi:10.1016/j.ijhydene.2011.07.034
- Weil, R., & Parker, K. (1990). The properties of electroless nickel. *Electroless Plating*, 111–137.
- Zhang, X., Wang, H., Scattergood, R. O., Narayan, J., & Koch, C. C. (2003). Evolution of microstructure and mechanical properties of in situ consolidated bulk ultra-fine-grained and nanocrystalline Zn prepared by ball milling, 344, 175–181.
- Zhou, F., Liao, X. Z., Zhu, Y. T., Dallek, S., & Lavernia, E. J. (2003). Microstructural evolution during recovery and recrystallization of a nanocrystalline Al-Mg alloy prepared by cryogenic ball milling, 51, 2777–2791. doi:10.1016/S1359-6454(03)00083-1